OPTICAL AND ELECTROCHEMICAL PROPERTIES OF BENZOTRIAZOLE AND BENZODITHIOPHENE CONTAINING ALTERNATING COPOLYMERS

A THESIS SUBMITTED TO
THE GRADUATE SCHOOL OF NATURAL AND APPLIED SCIENCES
OF
MIDDLE EAST TECHNICAL UNIVERSITY

BY

MERVE YILDIRIM

IN PARTIAL FULFILLMENT OF THE REQUIREMENTS
FOR
THE DEGREE OF MASTER OF SCIENCE
IN
CHEMISTRY

FEBRUARY 2021

Approval of the thesis:

OPTICAL AND ELECTROCHEMICAL PROPERTIES OF BENZOTRIAZOLE AND BENZODITHIOPHENE CONTAINING ALTERNATING COPOLYMERS

submitted by **MERVE YILDIRIM** in partial fulfillment of the requirements for the degree of **Master of Science in Chemistry, Middle East Technical University** by,

Prof. Dr. Halil Kalıpçılar
Dean, Graduate School of **Natural and Applied Sciences** _____

Prof. Dr. Özdemir Doğan
Head of the Department, **Chemistry** _____

Prof. Dr. Ali Çırpan
Supervisor, **Chemistry, METU** _____

Examining Committee Members:

Prof. Dr. Levent Kamil Toppare
Chemistry, METU _____

Prof. Dr. Ali Çırpan
Chemistry, METU _____

Prof. Dr. Yasemin Arslan Udum
Technical Science Vocational School, Gazi University _____

Assoc. Prof. Dr. İrem Erel Göktepe
Chemistry, METU _____

Assoc. Prof. Dr. Emrullah Görkem Günbaş
Chemistry, METU _____

Date: 15.02.2021

I hereby declare that all information in this document has been obtained and presented in accordance with academic rules and ethical conduct. I also declare that, as required by these rules and conduct, I have fully cited and referenced all material and results that are not original to this work.

Name, Last name : Merve Yıldırım

Signature :

ABSTRACT

OPTICAL AND ELECTROCHEMICAL PROPERTIES OF BENZOTRIAZOLE AND BENZODITHIOPHENE CONTAINING ALTERNATING COPOLYMERS

Yıldırım, Merve
Master of Science, Chemistry
Supervisor : Prof. Dr. Ali Çırpan

February 2021, 83 pages

The demands of humanity are changing and enhancing day by day with the increasing population. One of the most significant needs is energy in the world; but not only energy is a requirement, but also green energy is a necessity due to global pollution. As a result, organic photovoltaic devices have been developed and investigated in recent years. In this study, two new donor-acceptor (D-A) type copolymers with different π-bridges were designed and synthesized for organic photovoltaic devices. In this study, polymers contain benzotriazole moiety as the acceptor unit, alkoxyphenyl substituted benzodithiophene moiety as the donor unit with selenophene and thiophene as the π-bridges were synthesized. The characteristic features of synthesized polymers P1 and P2 were investigated via electrochemical, optical, spectroelectrochemical and kinetic studies. The optical band gaps were found as 1.83 eV and 1.81 eV for P1 and P2, correspondingly. Moreover, HOMO and LUMO energy levels of P1 were recorded as -5.25 eV/ -3.34 eV; HOMO and LUMO energy levels of P2 were recorded as -5.38 eV/-3.48 eV, respectively. The electronic band gap (E_g^{el}) values of P1 and P2 were calculated as 1.91 eV and 1.90 eV. The polymers were used as the donor materials and $PC_{71}BM$ as the acceptor material in the active layer of bulk heterojunction organic

photovoltaic devices. The photovoltaic features of P1 and P2 based organic solar cells were examined ITO/PEDOT:PSS/Polymer:PCBM/LiF/Al device structure and measured under standard AM 1.5 G illumination (100 mW/cm^2). The highest power conversion efficiency was recorded as 1.40% with a J_{SC} of 4.39 mA/cm^2, a V_{OC} of 0.71 V and a FF of 45% for P1. The highest power conversion efficiency of bulk heterojunction solar cell device based on P2 was recorded as 3.57% with a J_{SC} of 9.67 mA/cm^2, a V_{OC} of 0.71 V and a FF of 52%.

Keywords: Benzotriazole, Benzodithiophene, Organic Photovoltaic Device, Stille cross-coupling reaction

ÖZ

BENZOTRİAZOL VE BENZODİTİYOFEN İÇEREN ALTERNATİF KOPOLİMERLERİN OPTİK VE ELEKTROKİMYASAL ÖZELLİKLERİ

Yıldırım, Merve
Yüksek Lisans, Kimya
Tez Danışmanı: Prof. Dr. Ali Çırpan

Şubat 2021, 83 sayfa

İnsanlığın talepleri artan nüfusla birlikte her geçen gün değişmekte ve artmaktadır. Dünyadaki en önemli ihtiyaçlardan biri enerjidir; ancak sadece enerji değil, küresel kirlilik nedeniyle yenilenebilir enerji de bir zorunluluktur. Sonuç olarak, organik fotovoltaik cihazlar son yıllarda geliştirilmekte ve araştırılmaktadır. Bu çalışmada, organik fotovoltaik cihazlarda kullanılması için farklı π-köprülere sahip iki yeni donör-akseptör (D-A) tipi kopolimer tasarlanmış ve sentezlenmiştir. Bu çalışmada, akseptör ünitesi olarak benzotriazol, donör birim olarak alkoksifenil ikameli benzoditiyofen, π-köprüleri olarak da selenofen ve tiyofen içeren polimerler sentezlenmiştir. Sentezlenen polimer P1 ve P2'nin karakteristik özellikleri elektrokimyasal, optik, spektroelektrokimyasal ve kinetik çalışmalarla araştırılmıştır. Optik bant boşlukları P1 ve P2 için 1.83 eV ve 1.81 eV olarak bulunmuştur. Ayrıca, P1'in HOMO ve LUMO enerji seviyeleri -5.25 eV/ -3.34 eV olarak kaydedilmiştir; P2'nin HOMO ve LUMO enerji seviyeleri sırasıyla -5.38 eV/ -3.48 eV olarak kaydedilmiştir. P1 ve P2'nin elektronik bant aralığı değerleri 1.91 eV ve 1.90 eV olarak hesaplanmıştır. Polimerler, yığın heterobağlantılı organik fotovoltaik cihazların aktif katmanında donör malzemeler olarak ve $PC_{71}BM$ akseptör malzeme olarak kullanılmıştır. P1 ve P2 tabanlı organik güneş pillerinin

fotovoltaik özellikleri ITO / PEDOT: PSS / Polimer: PCBM / LiF / Al cihaz yapısı ve standart AM 1.5 G aydınlatma (100 mW / cm^2) altında incelenmiş ve ölçülmüştür. En yüksek güç dönüştürme verimi P1 için 4.39 mA/cm^2 J_{SC}, 0.71 V V_{OC} ve % 45 FF değerleri ile % 1,40 olarak kaydedilmiştir. P2 içeren yığın heterobağlantılı güneş pili cihazının en yüksek güç dönüşüm verimliliği, 9.67 mA/cm^2 J_{SC}, 0.71 V V_{OC} ve % 52 FF değerleri ile % 3.57 olarak kaydedilmiştir.

Anahtar Kelimeler: Benzotriazol, Benzoditiyofen, Organik Fotovoltaik, Stille çapraz kenetlenme reaksiyonu

To my beloved grandmother…

ACKNOWLEDGMENTS

First and foremost, my sincere gratitude to my supervisor Prof. Dr. Ali Çırpan for the opportunity to work in his group and his guidance, advice, endless patience during my thesis study.

I would like to thank Prof. Dr. Levent Toppare for his guidance and scientific support throughout this master study.

I am grateful to Asst. Prof. Dr. Şerife Özdemir Hacıoğlu for her help in electrochemical studies and her guidance. I would like to thank Mert Can Erer for his help in photovoltaic studies.

I sincerely thank Şevki Can Cevher and Sultan Taşkaya Aslan for their endless support, guidance, and patience. Their knowledge and expertise save me and my experiments most of the time.

I would also thank Meriç Çalışkan and Gülten Özkul Atlı for their great friendships. Everytime I fell, they were there for me. I could not express my feelings to have you. I will always be there whenever you need me till death tear us apart.

I am grateful to my labmates Yeliz, Duygu, Berrin, Yeşim, Ali Sait, Dilan Ece, Oğuzhan, Selin, Aslı for their friendships and peaceful laboratory environment.

I am grateful to three mood shifters of mine; Ozan Ünver, Aylin Elçi and İrem Akkan for their friendships, encouragement, tolerance and motivations. When I was not in a happy place, you were the ones who make me laugh.

I sincerely thank Pelin Akman Çolak for her help, support and motivation during writing the thesis.

Finally, I would like to thank my family for their endless love, patience, and tolerance. I love you to the moon and back.

This study supported by the Scientific and Technological Research Council of Turkey (TUBITAK) (Project numbers: 115M036, 118Z067, 115F604).

TABLE OF CONTENTS

APPENDICES

LIST OF TABLES

TABLES

LIST OF FIGURES

FIGURES

LIST OF ABBREVIATIONS

ABBREVIATIONS

ACN	Acetonitrile
AFM	Atomic force microscopy
Ag	Silver
AI	Aluminum
AM1.5G	Air mass 1.5 global
BDT	Benzodithiophene
BHJ	Bulk heterojunction
BLA	Bond length alternation
BTz	Benzotriazole
CB	Conduction band
$CHCI_3$	Chloroform
CE	Counter electrode
CP	Conjugated polymer
CV	Cyclic voltammetry
D-A	Donor-Acceptor
DCB	1,2-dichlorobenzene
DIO	1,8-diiodooctane
DSC	Differential scanning calorimetry

ECD	Electrochromic device
E_g	Band gap
E_g^{el}	Electronic band gap
E_g^{op}	Optical band gap
EQE	External quantum efficiency
ETL	Electron transport layer
eV	Electron volt
FF	Fill factor
GPC	Gel permeation chromatography
HOMO	Highest occupied molecular orbital
HTL	Hole transport layer
ICT	Intramolecular charge transfer
ITO	Indium tin oxide
J_{max}	Maximum current density
J_{sc}	Short circuit current density
J-V	Current Density-Voltage
LiF	Lithium fluoride
LUMO	Lowest unoccupied molecular orbital
NIR	Near-infrared
OFET	Organic field effect transistor
OLED	Organic light emitting diode
OPV	Organic photovoltaic

OSC	Organic solar cell
PA	Polyacetylene
$PC_{71}BM$	Phenyl-C71-butyric acid methyl ester
PCE	Power conversion efficiency
PDI	Polydispersity index
PEDOT	polyethylenedioxythiophene
PEDOT:PSS	Poly(3,4-ethylenedioxythiophene)-Polystyrenesulfonate
P_{in}	Incident light power
P_{max}	Maximum power
PPP	Polyparaphenylene
PPy	Polypyrrole
PT	Polythiophene
Pt	Platinum
RE	Reference electrode
Rs	Series resistance
R_{sh}	Shunt resistance
$TBAPF_6$	Tetrabutylammonium hexafluorophosphate
TGA	Thermogravimetric analysis
THF	Tetrahydrofuran
UV-ViS	Ultraviolet-visible
VB	Valance band
V_{max}	Maximum voltage

V_{oc}	Open circuit voltage
WE	Working electrode

CHAPTER 1

INTRODUCTION

1.1. Conjugated Polymers

A macromolecule that consists of repeating small units is called as a polymer. Polymers were known as insulators and used for coating of copper wires. Shirakawa and his co-workers discovered conducting polymer in 1977 by doping polyacetylene (PA) with iodine vapor. In 2000, Alan G. Macdiarmid, Hideki Shirakawa and Alan J. Heeger rewarded The Nobel Prize in Chemistry with this study. This breakthrough discovery put a different new complexion on conductive polymers [1]. After the discovery of conductive polymer, new conductive polymers were synthesized and recorded. These findings opened a new era in industrial and academic studies [2].

Conjugated Polymers (CPs) have alternating double and single bonds in their backbones, and π electrons' delocalization leads to conduct electricity [3]. CPs have been used in applications of organic field effect transistors, electrochromic devices, organic light emitting diodes and organic solar cells since they have many advantages such as ease to process, low cost, ease in band gap tunability [4]. Some examples of widely used conjugated polymers such as polyacetylene, polyethylenedioxythiophene, polythiophene, polypyrrole, polyphenylene were shown in Figure 1.1.

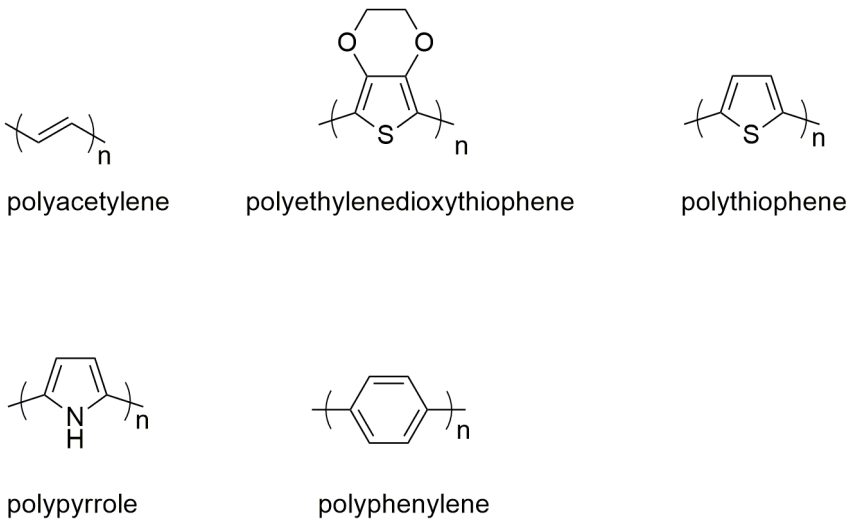

Figure 1.1. Some examples of widely used CPs

1.2. Doping Process

The neutral state of conjugated polymers is non-conductive. For the conduction of electricity, the doping process, achieved by electrochemical or chemical doping, is crucial to introduce mobile charge carriers. Chemical doping is a method that depends on a chemical reaction between CPs with an oxidizing or reducing agent, while the electrochemical doping process relies on oxidation or reduction of the polymer by applying voltage [5].

If electrons are removed from HOMO of CPs, the mechanism is called p-doping. In contrast, the process is called n-doping if the electrons' donation to LUMO state of the conjugated polymer is happened [6]. Schematic representation of p-doping and n-doping processes were illustrated in Figure 1.2.

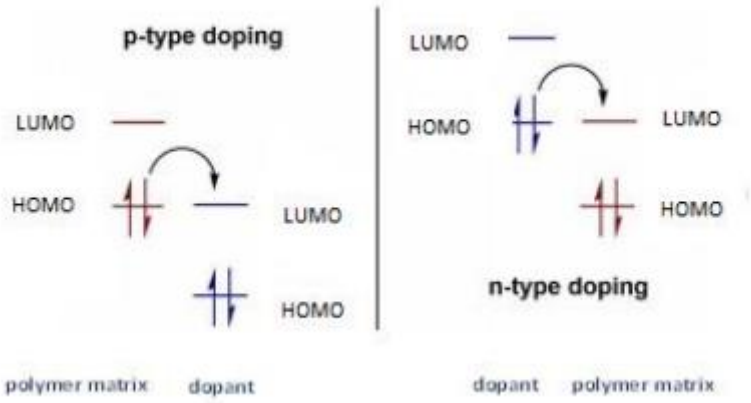

Figure 1.2. Scheme of p-doping and n-doping processes

Polaron, bipolaron, and soliton are formed as a result of the doping process. The radical anion or cation which are formed during the doping process is called polaron. By the further ionization, the formation of dianions or dications which are called bipolarons is observed. These observed defects lead to generating charge carriers; thus doping process is crucial to achieving high conductivity [7], [8]. The presented neutral state, polaron and bipolaron state of polythiophene were depicted in Figure 1.3.

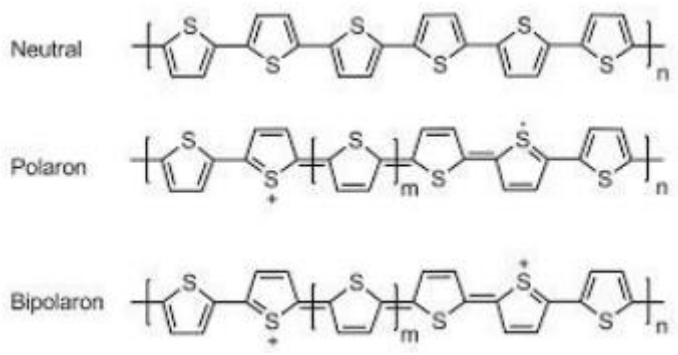

Figure 1.3. The neutral state, polaron and bipolaron state of polythiophene

1.3. The Band Theory

The band gap is the term that is defined as the energy difference between the valance band (VB) and the conduction band (CB) of materials. For the conjugated polymers, HOMO is represented by the valance band; while, LUMO is represented by the conduction band. Therefore, the band gap of a material is directly related to its conductivity level. Materials can be classified as insulators, semiconductors or metals regarding their conductivity. Electronic band structures of insulators, semiconductors and metals are illustrated in Figure 1.4.

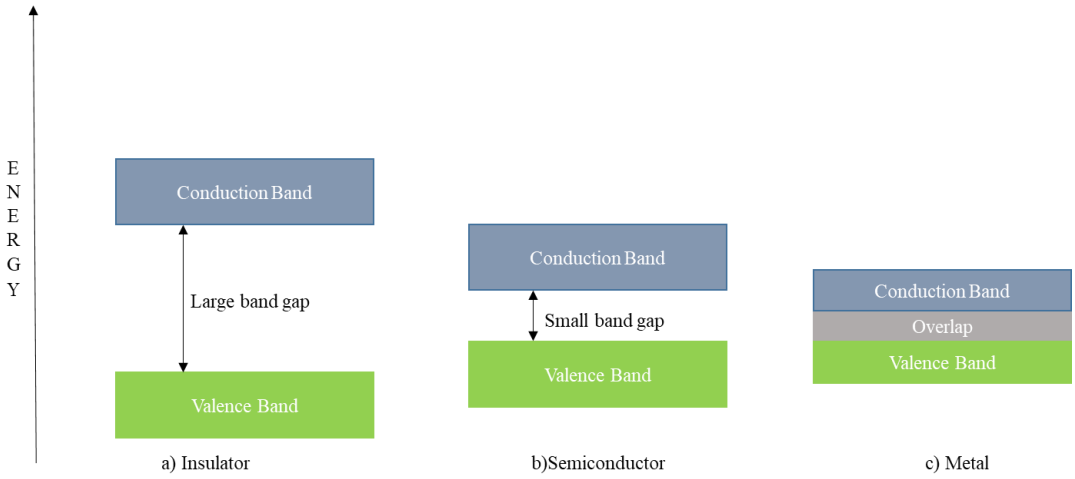

Figure 1.4. Electronic band structures of a)insulators, b)semiconductors and c)metals

For metals, there is no energy difference between the valance band and the conduction band. The overlap between these bands supply that valence electrons can migrate freely to the conduction band. Therefore, the conductivity feature of metals is great. For insulators, the energy difference between VB and CB is too vast for the migration of electrons. Since electrons cannot travel from the valance band to the

conduction band, the insulators cannot conduct electricity. The band gap of semiconductors is between conductors and insulators, so excited electrons can transport from VB to the CB. Conductive polymers are considered as semiconductors and a narrow band gap of conductive polymers helps the movement of electrons along the polymer chain [9].

1.4.Band Gap Engineering

The band gap of a conjugated polymer has great importance in organic photovoltaic application since it influences the optical and electrical properties of the polymer. Band gap engineering is the procedure of modifying the band gap of the conductive polymer by making adjustments in parameters such as planarity (E_θ), substituents (E_{Sub}), aromaticity (E_{Res}), bond length alternation (E_{BLA}) and intermolecular interactions (E_{Int}) [10], [11]. As a result, the band gap of the conjugated system can be denoted by the following formula;

$$E_g = E_\theta + E_{Sub} + E_{Res} + E_{BLA} + E_{Int}$$

Conductive polymers have two resonance structures with different band gaps namely aromatic and quinoid forms for their non-degenerate ground state. Aromatic form is provided with confined π-electrons. The π-electrons are delocalized through the polymer chain and cause the formation of quinoid form. Lower stability and smaller band gap are observed for the quinoid resonance structure over the aromatic resonance structure. The ratio between aromatic to quinoid population can be affiliated with bond length alternation. Also, the more aromatic population in the ground state refers to higher BLA, so higher band gap. Conversely, a higher population of quinoid form in the ground state refers to less BLA, thus lower band gap [10], [12].

Enhancement of conjugation and delocalization of polymer chain provides a lower band gap. To achieve this, planarity should be fixed up. Since parallel π orbitals interactions enlarge the length of conjugation and enable delocalization, planarity decreases; thus, the band gap is reduced [13].

The introduction of substituents to the polymer matrix is one of the most effective ways to decrease the band gap. When electron donating groups are attached to the polymer backbone, it raises the HOMO energy level. On the contrary, attachment of the electron withdrawing groups lowers the LUMO energy level. Thus, the substitution of electron withdrawing or electron acceptor groups to the polymer chain leads to a narrower band gap.

Another factor that is vital to modify the band gap of conjugated polymer is the intermolecular interactions. The solid-state of polymers has a lower band gap compared to solution-state due to more crystalline and rigid structure which leads to improvement in intermolecular interactions and π-π stacking [14]–[16].

1.5.Donor-Acceptor Approach in Conjugated Polymers

As mentioned before to get narrow band gap is crucial for the optoelectronic properties of conjugated polymers. The polymers having narrow band gaps provide absorbing broader scale of solar spectrum which especially perform absorbing photons in the near-IR region. In order to obtain high performance organic photovoltaics, these polymers are required to be designed and synthesized. In recent years, the most prevalent method to design conjugated polymers having low band gap is the donor-acceptor (D-A) approach which consists of repetitive alternating conjugated donor (D) and conjugated acceptor (A) units in the same main chain of copolymer. In 1993, Havinga and his co-workers suggested a theory about decreasing the band gap via hybridization of molecular orbitals of polymers [17]. In this approach, alternating electron acceptor with low LUMO and electron donor moieties with higher HOMO are combined in the polymer chain and a new low band

gap via interchain charge transfer is produced [17]. This approach not only provides a lower band gap but also enlarges the electrochemical and optical features with improved charge mobility and wavelength absorption [18], [19]. The new HOMO and LUMO levels and band gap for donor-acceptor containing polymer were depicted in Figure 1.5.

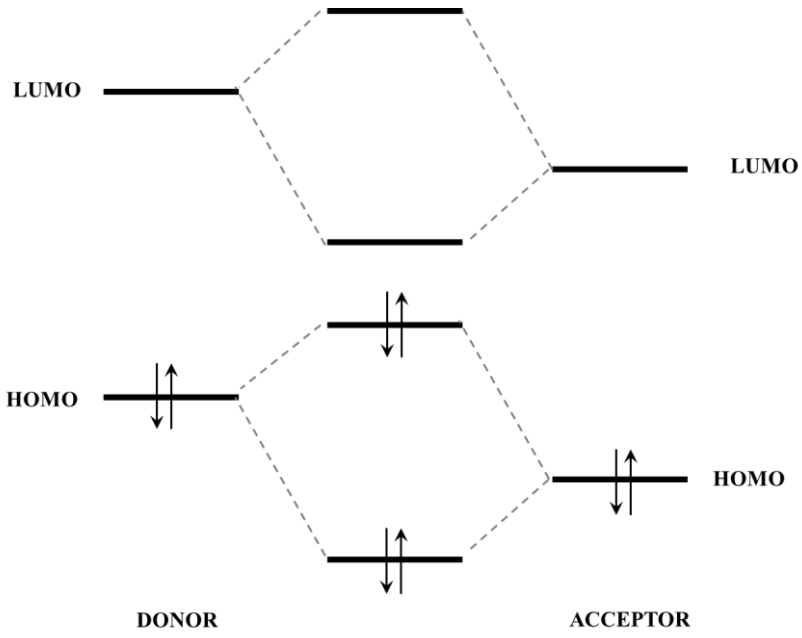

Figure 1.5. Creation of new molecular orbital energy diagram in D-A approach

1.6. Moieties in Donor-Acceptor Type Conjugated Polymers

1.6.1. Benzotriazole Moiety

Benzotriazole (BTz) has drawn attention under the electron acceptor unit's categorization by reason of its electron deficient structure and its stability. The first benzotriazole containing polymer was synthesized in 2006 by Yamamoto and Tanimoto [20]. The molecular structure of benzotriazole moiety is depicted in Figure

1.6. Due to diimine bonds in its molecular structure, BTz has a great electron deficient property and also has a low lying LUMO level. Moreover, the solubility of the polymer containing the BTz unit can be improved by the attachment of alkyl groups on nitrogen position. Thanks to these unique properties, benzotriazole bearing polymers have been utilized in many application areas such as electrochromic devices, organic light emitting diodes, organic solar cells and organic field effect transistors [21], [22].

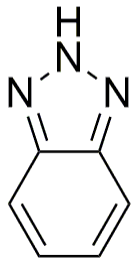

Figure 1.6. Chemical structure of benzotriazole

1.6.2. Benzodithiophene Moiety

Benzodithiophene contains a benzene ring with coherent thiophene which constitutes a planar and symmetric molecular structure. The molecular structure of the benzodithiophene unit is represented in Figure 1.7. This unique molecular structure gives BDT to great electron donor ability with low HOMO level. In addition, having planar and symmetric structure of BDT unit leads increase in generation of π-π stacking that provides high charge carrier mobility owing to easy generation of π-π stacking. Moreover, alkyl or alkoxy substitution to benzodithiophene unit provides increment in solubility of the polymer [23], [24].

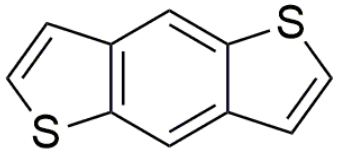

Figure 1.7. Chemical structure of benzodithiophene

1.6.3. Moieties of π-Bridges: Thiophene and Selenophene

The electron donor π-bridges have been widely utilized to obtain higher efficiencies in photovoltaic applications. Introducing π-bridges between acceptor and donor units improves the planarity and reduces the polymer chain's steric hindrance. The most commonly used heterocyclic π-bridges are selenophene and thiophene [15].

Thiophene has higher aromaticity than selenium containing analog, so selenophene has a more stable quinoid form, leading to extended conjugation length of conjugated polymers and a wider absorption band in the spectrum. Additionally, the improved charge carrier mobility and lowered band gap are caused by the fact that the selenium atom's polarizability is higher than the sulfur atom. On the other hand, the more soluble nature of thiophene is caused by the rigidity of selenium containing selenophene [25], [26].

Figure 1.8. Chemical structure of thiophene and selenophene

1.7. Organic Photovoltaics

Organic photovoltaics are devices that create electricity via absorbing sunlight. Unlike their inorganic counterparts, organic photovoltaics possess features like easy and low-cost production, flexibility and exhibiting high absorptivity [27]–[29]. For all these characteristic properties, organic photovoltaics has drawn attention in both academic and industrial environments. However, the low power conversion efficiency of organic semiconductors is the main handicap [30]. For increasing efficiency, the scientists develop and construct different organic solar cell structures such as bulk heterojunction, bilayer and single layer organic solar cells.

The first and simplest construction of organic solar cell is named as single layer organic photovoltaics which consist of a single organic layer placed between two electrodes [27]. The power conversion efficiencies of these devices were very low due to low charge collection and exciton dissociation. In 1986, C. Tang and his-coworkers was constructed bilayer organic solar cells with 1% PCE [31]. Bilayer OPVs have consisted of donor and acceptor organic semiconductor material which has similar working principles with p-n junction inorganic solar cells. However, these types of organic photovoltaics had some drawbacks such as the exciton recombination and not having adequate thickness for the absorption of light [27]. To overcome these drawbacks, bulk heterojunction (BHJ) organic solar cell architecture was introduced by Yu and his co-workers [32]. In bulk heterojunction organic devices, the donor and acceptor materials were blended to obviate charge recombination and the low charge generation [33]. The representation of active layers of single layer, bilayer and BHJ organic photovoltaic cell was illustrated in Figure 1.9.

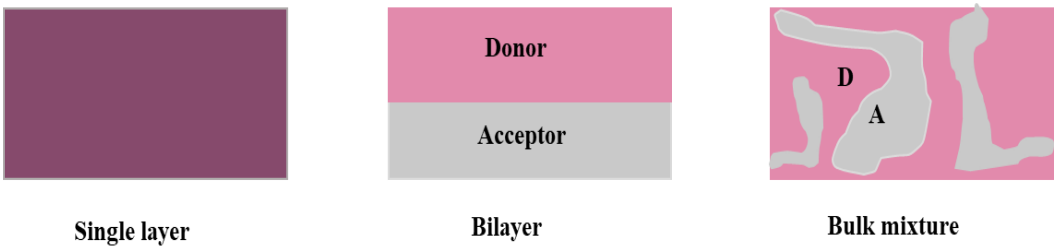

Figure 1.9. Representation of active layer of single layer, bilayer and BHJ organic photovoltaic devices

1.7.1. Device Construction of Bulk Heterojunction Organic Photovoltaics

To accomplish the highly performed organic solar cells, various necessities should be achieved by proper device construction. These requirements include efficient light absorption via donor moiety, a tremendous amount of charge carrier creation and excellent transportation and collection of these carriers. Bulk heterojunction organic photovoltaics consist of an active layer where donor and acceptor material is blended with multilayered construction. Device construction of BHJ solar cells involves a few steps starting with coating of a glass substrate. This is achieved by indium tin oxide (ITO), conductive and transparent material serving as an anode. The anode materials should be chosen from properties such as high conductivity, great stability and also good film formability. Then, coating of the hole transport layer consisting of poly(3,4-ethylenedioxythiophene):polystyrene sulfonate (PEDOT:PSS) is achieved by spin coating technique. The hole transport layer provides ITO to diminish its work function and smoothen its surface. In addition to these, HTL provides OPVs to transport and collect positive charge carriers easily and block the flow of electrons to the anode. Active layers which contains donor-acceptor blend were deposited onto the hole transport layer. Active layer comprises blending of donor and acceptor materials - the blend of organic conjugated polymer as a donor moiety and acceptor material like fullerene derivatives. With the help of this blended active layer, the exciton traveling distance is reduced. Therefore, the charge separation

feature of the device is enhanced and could be processed anywhere in the active layer. Lithium fluoride (LiF) and aluminum (Al) are deposited as the final step to construct the bulk heterojunction solar cell where LiF works as an electron transport layer and Al work as the cathode. The bulk heterojunction device construction can be seen in Figure 1.10. The main functions of electron transport layer (ETL) can be explained as both extraction of electrons efficiently and restraining the reverse flow of positive charge carriers through the cathode. To obtain high performance OSC devices, ETL materials should be selected as regards their great electron transportation ability and also transparency features [34]–[36].

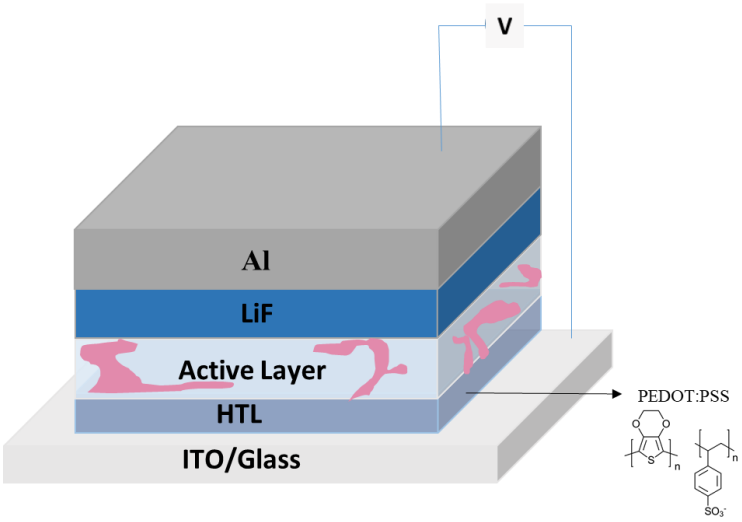

Figure 1.10. Device construction of bulk heterojunction organic photovoltaics

1.7.2. Working Principles of Bulk Heterojunction OPVs

The basic working mechanism of bulk heterojunction organic photovoltaics can be explained with four main steps to produce electricity from the absorption of light.

The first step is the absorption of incoming light and generation of bounded electron-hole pair which is called as exciton. Light absorption arouses excitation of electrons from the highest occupied molecule orbital (HOMO) to the lowest unoccupied molecule orbital (LUMO) and the holes which are the positive charge carriers stay in HOMO level. The electron and hole pair is bounded coloumbically and called as Frenkel exciton. Later, exciton diffuses to donor-acceptor interphase. After that, the exciton dissociates into free charges at donor-acceptor interphase, electrons and holes migrate to donor and acceptor phases separately. As a final step, free charges are collected at corresponding electrodes [37]–[40]. Schematic representation of the working mechanism of organic photovoltaics was illustrated in Figure 1.11.

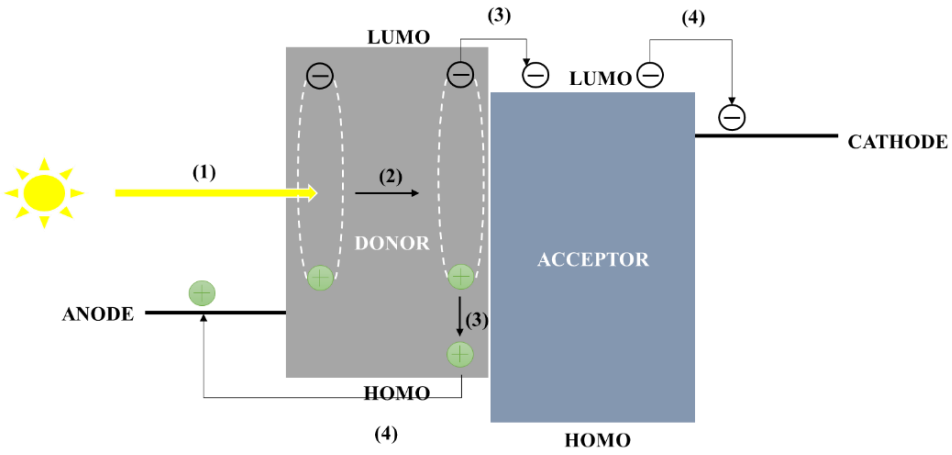

Figure 1.11. The basic working mechanism of organic photovoltaics

1.7.3. Characterization of Organic Photovoltaics

Photovoltaic parameters are obtained by current density (J)-voltage (V) curve with and without light as shown in Figure 1.12. Under dark conditions, there is no potential or current, so the curve passes through the origin. With illumination, the curve is located in the 4th quadrant which shows the generation of power [41]. The

efficiencies of solar cells or the power conversion efficiency can be calculated by dividing the maximum power obtained from the cell by the incident power. The PCE of organic solar cell is measured by the use of the J-V curve under standard conditions which is AM1.5 G with an intensity of 1000 watt/m^2 [42] and this term is formulated as follows;

$$FF = \frac{Vmax\ x\ Jmax}{Voc\ x\ Jsc}$$

$$PCE = \frac{Pmax}{Pin} = \frac{Voc\ x\ Jsc\ x\ FF}{Pin}$$

Where J_{sc} is a short circuit, V_{oc} is open circuit voltage, FF is fill factor, P_{max} is the maximum power and P_{in} is the power of the incident light.

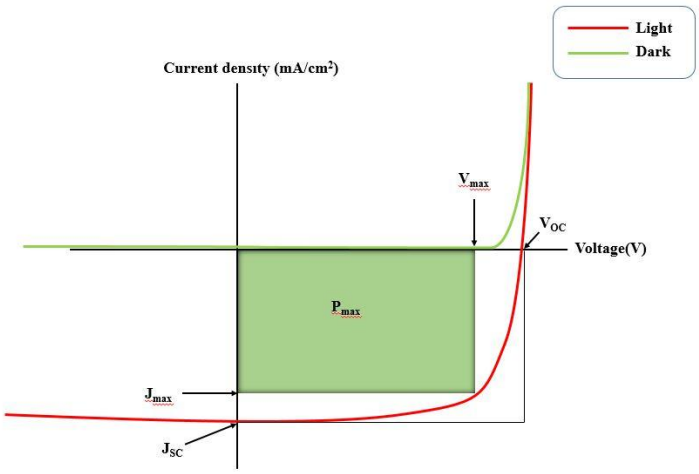

Figure 1.12. Current density (J)-voltage (V) curve under dark and light

The calculations of power conversion efficiencies of devices are done under Air Mass 1.5 Global (AM1.5 G). The standardization of air mass is necessary to

characterize the photovoltaics. It should be considered as the spectrum of radiation, not the intensity of light. AM1.5 G is identified as the radiation of sunlight, which crossed the earth's surface at an angle with 48°. AM1.5 G with 100 mW/cm^2 is applied for the characterization of solar cells [43]. AM1.5 Global Standardization is represented in Figure 1.13.

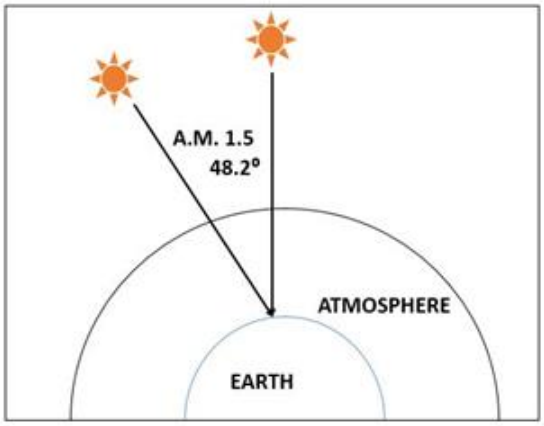

Figure 1.13. Representation of AM 1.5 global standardization

1.7.4. Basic Parameters Affecting Organic Photovoltaics

1.7.4.1. Open Circuit Voltage

The value of open circuit voltage (V_{OC}) is obtained from an illuminated PV system when no current passes through the cell. Therefore, V_{OC} can also be defined as the potential difference between cathode and anode caused by free charge migration. In a mathematical way, V_{OC} is easily calculated by the below equation;

$$V_{OC} = \frac{1}{e}(E_{DONOR}\ HOMO - E_{ACCEPTOR}\ LUMO) - 0.3\ V$$

Where E_{DONOR} HOMO shows the donor's HOMO energy level, $E_{ACCEPTOR}$ LUMO shows the acceptor's LUMO energy level and e stands for the elementary charge. As seen in the equation, V_{OC} is directly related with the HOMO energy level of donor and LUMO energy level of acceptor with a deviation of 0.3 V. This mathematical formula was initially established by associating the energy difference HOMO energy level of the donor, the LUMO energy level of the acceptor in bulk heterojunction photovoltaics construction with different polymers. The deviation obtained by comparing the band gaps of BHJ materials with the open circuit voltage measured at room temperature is due to the temperature dependence of the quasi-Fermi levels in fullerene and the polymer [44]. The recombination process causes low open circuit voltage. To avoid recombination of electrons and holes and to obtain high V_{OC}, the device should have the optimum morphology [45].

1.7.4.2. Short Circuit Current Density

The value of short circuit current density (J_{SC}) can be obtained from an illuminated PV system when external voltage does not exist. J_{SC} is directly related to solar cell efficiency because it is defined as the production and collection of light generated charge carriers. The fundamental equation of short circuit current density is given below;

$$J_{SC} = neE\mu$$

Where n is the charge carrier density, e refers to the elementary charge, E refers to the generated electric field and μ stands for the charge carrier mobility. The J_{SC} relies on the charge carrier mobility which is mostly affected by the morphology of the active layer and collection of charges. Moreover, J_{SC} depends on the active layer's

absorption coefficients, the diffusion efficiency of the excitons, the absorbed light intensity, the transport and the collecting efficiencies of the charge carriers [46].

One of the most critical parameters that reveal the energy conversion features of the organic solar cells is called as external quantum efficiency (EQE). This term can be defined as the ratio of the number of charge carriers collected by the solar cell to number of incident photons. The EQE measurement gives an opportunity to observe behaviours of solar cells in a specific wavelength. The EQE is proportional to J_{SC} of the cell and intensity of incident light (J_I) at specific wavelength (λ) [47]. It is important to note that EQE value is equal to unity for an ideal case. Below formulation represents the EQE and its dependency of mentioned parameters where the h is the Planck constant and c is the speed of light;

$$\text{EQE}\ (\lambda) = \frac{J_{SC}\ (\lambda)}{J_{I\ (\lambda)}}\, x\, \frac{hc}{\lambda}$$

1.7.4.3. Fill Factor

The quality identification of the solar device is generally determined by a parameter namely fill factor and this term is briefly defined as squareness of a J-V curve. It was formulated with an equation which the ratio of maximum power to V_{OC} and J_{SC} values as shown below;

$$\text{FF} = \frac{Vmax\ x\ Jmax}{Voc\ x\ Jsc}$$

The fill factor (FF) is associated with two main factors in the circuit of solar cell devices, which are called as shunt resistance (R_{sh}) and series resistance (R_s). As mentioned before, the maximum power of organic solar cells originated from the device with an illumination equal to J_{SC} multiply to V_{OC}. Hence, the rectangular shape is generated as a result from current density-voltage curve of the device. On the contrary to the ideal situation, in general P_{max} is limited to the multiplication of J_{max} and V_{max}. The reason for this, in practice, there are undesirable conditions such as recombination of charge carriers and diode deviations from an ideal situation where series resistance is zero while shunt resistance goes to infinity. The series resistance (R_s) is the term that can be explained as a factor relating to the mobility properties of charge carriers. In the conditions where traps exist in the solar cell device, charge carriers will decline due to an increase in travel distance for them. In addition, the shunt resistance (R_{sh}) can be described as the term is related to the recombination of charge carriers at nearly interface of donor and acceptor. When a decrease in shunt resistance of the device is occured the current finds a different pathway to pass which causes declining the current flow throughout the organic solar cell device [38], [48], [49]. Thus, low R_s and high R_{sh} values were required to obtain high FF and high PCE values.

1.8. Literature Studies of Benzodithiophene Containing Organic Photovoltaics

Among the literature studies, benzodithiophene (BDT) derivatives are seen as one of the most essential electron-donating moieties for π-conjugated copolymers in order to be utilized in organic solar cell applications with high power conversion efficiency (PCE). The high amount of electron delocalization is provided with BDT derivatives because it has a high degree of planar and fused structure which could improve the charge carrier mobility. Furthermore, stronger inter-chain and broader absorption of light properties are achieved thanks to its excellent structural properties. In addition to these, side chain substitution is achieved easily to BDT structure. In 2014, Ünay et. al. synthesized 4,7-Bis(5-bromoselenophen-2-yl)-2-(2-octyldodecyl)-2H-

benzo[d][1,2,3]triazole and 2,6-bis(trimethylstannyl)-4,8-bis(2-ethylhexyloxy)benzo[1,2-b:4,5-b′]dithiophene containing conjugated alternating copolymer P-SBTBDT (Figure 1.14) in which selenophene was used as π-spacer. P-SBTBDT showed an electronic band gap of 1.83 eV with HOMO energy level of -5.17 eV and LUMO energy level of -3.34 eV. PSBTBDT: $PC_{71}BM$ based bulk heterojunction solar cell exhibited 3.60% PCE. V_{OC}, J_{SC} and FF values of the BHJ solar cell was reported as 8.95 mA/cm^2,0.67 V, 60% [50].

Recently, the fluorinated alkoxy phenyl substituted benzodithiophene as electron rich donor moiety have been studied. With the introduction of phenyl group having high ionization energy, lowering of HOMO energy levels and increasing of the V_{OC} value are provided. Besides, with the fluorinated alkoxylphenyl substitution to BDT unit, reaching the deeper HOMO energy levels for the higher photovoltaic performance can be provided.

In recent years, various studies have reported that designing fluorinated alkoxyphenyl side chain based BDT containing polymers as electron rich moiety coupled with the polymers having high electron accepting properties have become widespread to reach the high power conversion efficiency (PCE) for the BHJ organic solar cells. In 2015, Yuan et al. published the article stated that bis(trimethyltin)-4,8-bis(4-ethylhexyloxy-1-meta-fluorophenyl)-benzo[1,2-b:4,5-b']-dithiophene and 4,7-di(5-bromothien-2-yl)-5,6dioctyloxybenzo[c][1,2,5]-oxadiazole containing conjugated alternating copolymer in which thiophene was used as π-bridge in its backbone (PBO-m-FBO) (Figure 1.14) reached 8.0% PCE in BHJ organic solar cell application [51]. V_{OC}, J_{SC}, and fill factor values of PBO-m-FBO based BHJ organic photovoltaics were reported as 0.87 V, 14.3 mA/cm^2 and 64%, correspondingly by using PBO-m-FPO/$PC_{71}BM$ blend (1:2, w/w) (3% DIO). Moreover, in 2017, Cong et al. synthesized m-fluoro-p-(2-octyldodecaneoxyphenyl)-substituted benzo[1,2-b:4,5-b0]dithiophene as electron donating moiety and the lactam comprising dye isoindigo (IID) derivative as electron accepting unit containing π conjugated copolymer which was named mF-IID (Figure 1.14) with 2.5% PCE. mF-IID based organic BHJ solar cell exhibited V_{OC}, J_{SC}, and fill factor values as 0.88 V, 5.61

mA/cm^2 and 50.5%, respectively by constructing polymer/$PC_{71}BM$ blend (1:1, w/w) [52]. Furthermore, Shin et al. synthesized benzodithiophene derivative fluorinated in the meta positions of the phenyl side chain and difluoro-benzothiadiazole based alternating copolymer with introducing alkylated thiophene as π-bridge (PPh-m-F) (Figure 1.14) exhibited 6.62% PCE. V_{OC}, J_{SC}, and fill factor of the organic BHJ solar cell by utilizing PPh-m-F/$PC_{71}BM$ blends (1:1.2, w/w) (1.5% DIO) were reported as 0.91 V, 11.25 mA/cm^2 and 64.6%, respectively, in 2017 [53].

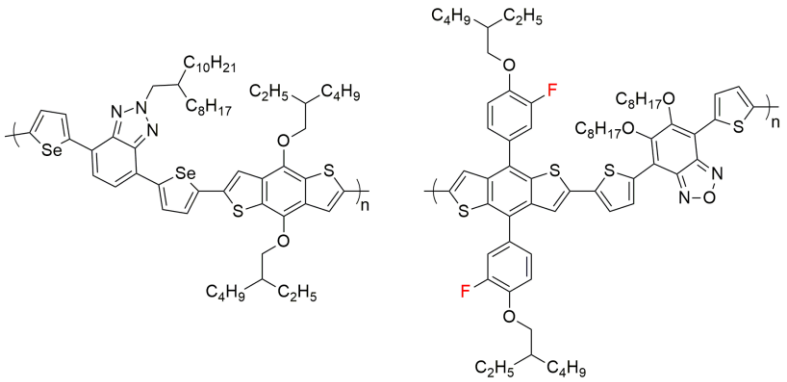

P-SBTBDT

PBO-m-FBO

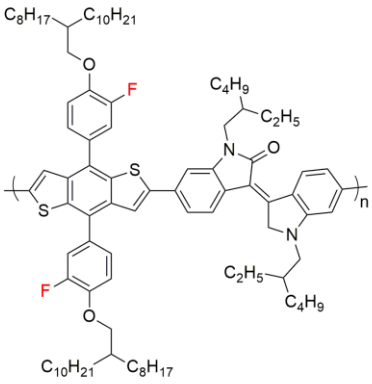

mF-IID

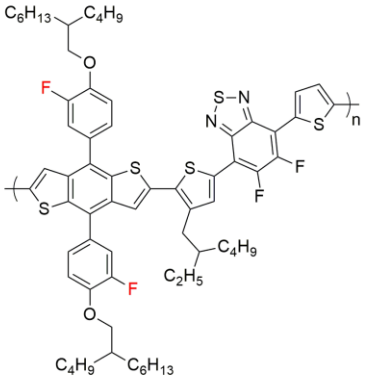

PPh-m-F

Figure 1.14. Molecular structures of BDT based P-SBTBDT, PBO-m-FBO, mF-IID and PPh-m-F

1.9. Aim of the Study

Recently, low band gap conjugated polymers have drawn attention in the academic environment due to their high photovoltaic efficiencies. The selection of donor and acceptor moieties has great importance because they affect the light absorption properties and the parameters of photovoltaic devices and tune HOMO-LUMO energy levels of the active layer of BHJ solar cells [54]. The narrow band gap (<2.0 eV) is vital to achieve high J_{SC} values so that high power conversion efficiencies [55]. However, too low band gap can cause low V_{OC}; hence low PCE [56]. For this reason, adjusting V_{OC} and J_{SC} values is crucial for the achievement of higher photovoltaic performance. The π-conjugated linkers strongly also affect the electronic structure of the polymer main chain and lower the band gap by enhancing the absorption towards the longer wavelengths. Moreover, as mentioned before, the F atom on the side chain of BDT unit increases the V_{OC} value by decreasing the HOMO energy level of the polymers [51]-[53]. In this study, the polymers containing different π-spacers are designed and synthesized by considering the reasons mentioned above to obtain high power conversion efficiencies. The molecular structure of polymers P1 and P2 were demonstrated in Figure 1.15 and Figure 1.16, respectively.

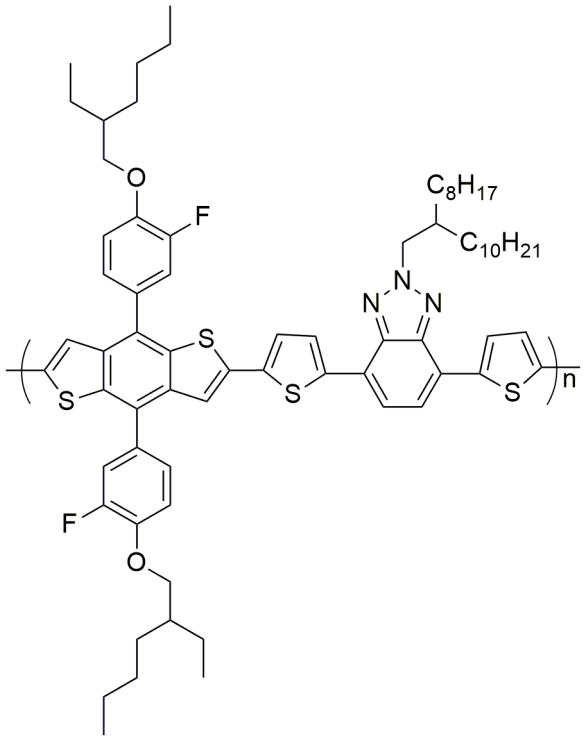

Figure 1.15. The molecular structure of thiophene containing P1

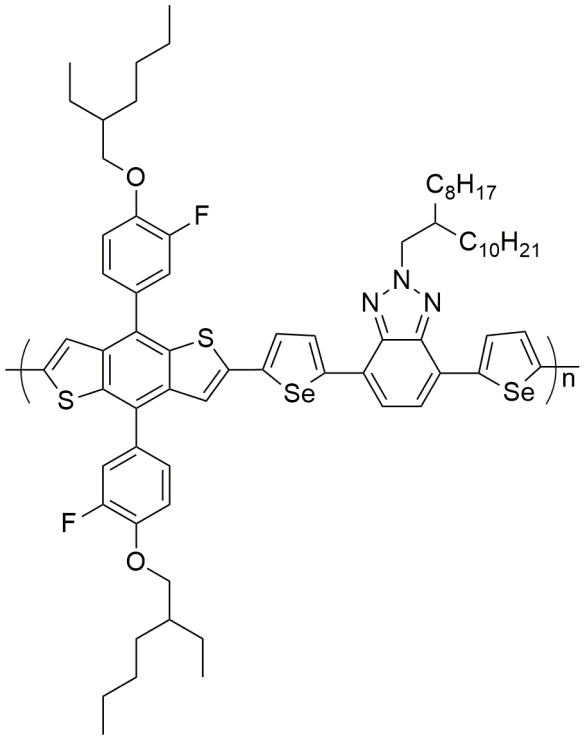

Figure 1.16. The molecular structure of selenophene containing P2

CHAPTER 2

EXPERIMENTAL

2.1. Materials and Equipment

Sigma Aldrich and TCI brand materials were purchased in order to synthesize the monomers and alternating copolymers. The reactions that have sensitivity for moisture and air were achieved under argon atmosphere. As the drying agent for THF and toluene, sodium and benzophenone ketyl were used; furthermore, other solvents were used without purification process. The silica gel was merchandized from Merck and utilized as the stationary phase in column chromatography in order to purify the synthesized crude products.

2.2. Synthesis of Monomers

2.2.1. Synthesis of 4,7-dibromobenzo[*c*][1,2,5]thiadiazole(2)

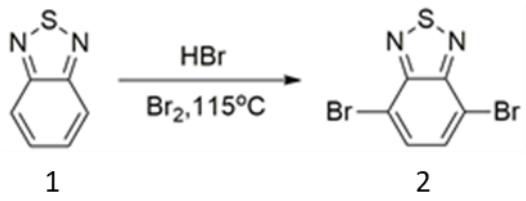

Figure 2.1. Synthesis of compound 2

At room temperature (RT), **compound 1** (5 g, 36.72 mmol) was dissolved in 60 mL HBr, following by adjusting the reaction temperature to 100 ℃ for one hour. After stirring the reaction mixture for an hour, bromine solution (18.2 g, 113.8 mmol) in 20 mL HBr was added drop by drop to the flask. The temperature of the solution was raised to 115 ℃. Then, the reaction mixture was allowed to be stirred overnight. The temperature of the reaction mixture was reduced to room temperature, following by adding 400 mL of saturated sodium bisulfate solution into the mixture. After that, the filtration with filter paper was done. The filtrate was washed with distilled water and cold ether. Yellow solid **compound 2** was obtained (9.4 g, 87.1%).

2.2.2. Synthesis of 3,6-dibromobenzene-1,2-diamine(3)

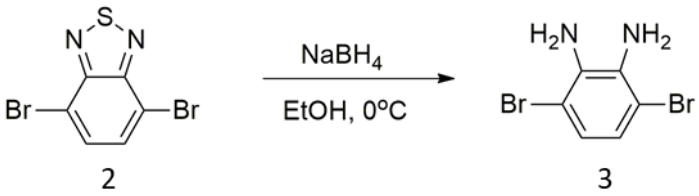

Figure 2.2. Synthesis of compound 3

Ethanol was used to dissolve **compound 2** (9.40 g, 31.98 mmol). The addition of $NaBH_4$ (24.2 g, 639.5 mmol) was performed when the temperature was lowered to 0 ℃. With the addition of sodium borohydride, the solution was taken to room temperature and was allowed to be mixed overnight. Later, the solvent evaporation was carried out with a rotary evaporator. The extraction of the crude product was performed with saturated salty water and ether. The organic phase was dried over Na_2SO_4. The disposal of the solvent was performed with a rotary evaporator to obtain the desired solid **compound 3**. (8.25 g, 97.0%).

2.2.3. Synthesis of 4,7-dibromo-2H-benzo[*d*][1,2,3]triazole(4)

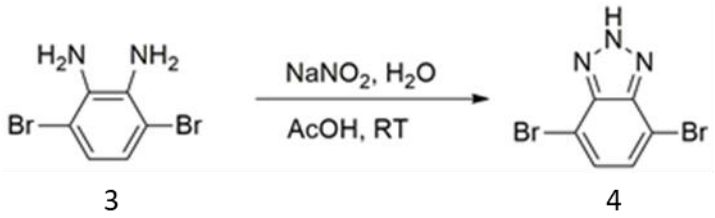

Figure 2.3. Synthesis of compound 4

Compound 3 (8.25 g, 31.02 mmol) was put in a flask with 100 mL acetic acid. Then, the reaction solution was stirred until compound 3 was completely dissolved at RT. After that, the solution that contains sodium nitrate (2.35 g, 34.13 mmol) with a sufficient amount of distilled water was poured into the flask slowly. The reaction mixture was allowed to be stirred for 2 hours. The solid product was washed with distilled water by suction filtration. Then, let it dry to get **compound 4** (5.52 g, 64.2%).

2.2.4. Synthesis of 4,7-dibromo-2-(2-octyldodecyl)-2H-benzo[*d*][1,2,3]triazole (6)

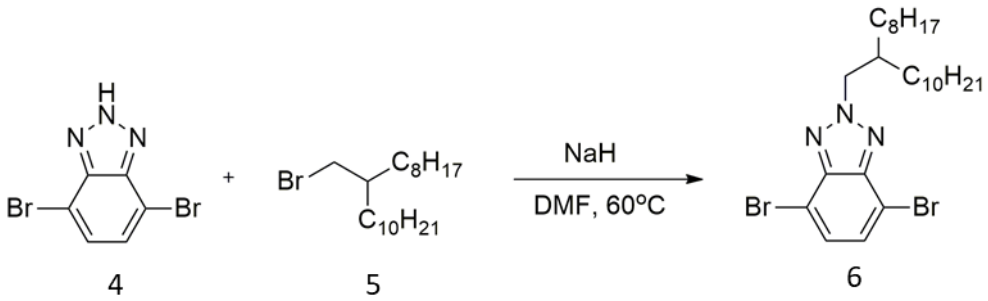

Figure 2.4. Synthesis of compound 6

Compound 4 (5.50 g, 19.86 mmol) was dissolved in 20 mL of dimethylformamide in an argon atmosphere. Afterward, NaH (0.57 g, 23.83 mmol) was put into the reaction medium at room temperature. After NaH was dissolved completely, the temperature of the medium was adjusted to 60 ℃. **Compound 5** (8.61 g, 23.83 mmol) was added to the reaction flask at once at that temperature. Then, the reaction mixture was stirred overnight. The extraction procedure was accomplished with distilled water and chloroform; then, a rotary evaporator was used to remove the solvent from the organic phase. Column chromatography was used for further purification of the crude product with hexane-chloroform mobile phase in the ratio of 4 to 1. Finally, **compound 6** was obtained (5.20 g, 47%).

^{1}H NMR (400 MHz, $CDCl_3$) δ 7.43 (s, 2H), 4.67 (d, J = 7.3 Hz, 2H), 2.38 – 2.30 (m, 1H), 1.30 – 1.19 (m, 32H), 0.86 (m, 6H).**^{13}C NMR** (100 MHz, $CDCl_3$) δ 143.52, 129.33, 109.87, 61.04, 38.90, 31.79, 31.74, 31.00, 29.65, 29.48, 29.35, 29.30, 29.21, 29.12, 25.88, 22.58, 22.54, 14.01.

2.2.5. Synthesis of tributyl(thiophen-2-yl)stannane(8)

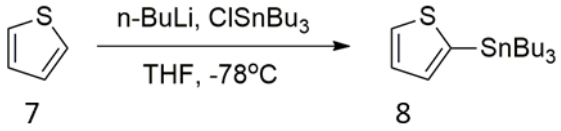

Figure 2.5. Synthesis of compound 8

Compound 7 (2.55 g, 30.31 mmol) was dissolved in 25 mL of dry THF, following by adjusting the reaction temperature to -78 ℃. At that temperature, the solution of n-BuLi (1.84 g, 2.5 M in hexane, 28.79 mmol) was put into reaction medium dropwisely. The reaction mixture was stirred at -78 ℃ one more hour. After that, the

addition of tributyltin chloride (10.85 g, 33.34 mmol) into the reaction mixture drop by drop was performed at the same temperature. After stirring one more hour under the same conditions, the reaction mixture was warmed to ambient temperature and was stirred overnight. Extraction of the crude product was performed with saturated salty water and diethyl ether; then, the organic phase was dried with a drying agent. There was no further purification step. The solvent was removed under reduced pressure in order to obtain **compound 8** (9.80 g, 87%).

2.2.6. Synthesis of 2-(2-octyldodecyl)-4,7-di(thiophen-2-yl)-2H-benzo[*d*][1,2,3] triazole(9)

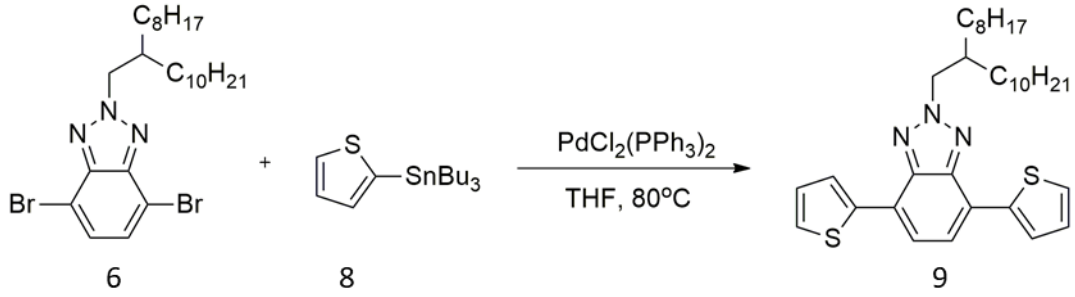

Figure 2.6. Synthesis of compound 9

Compound 6 (0.60 g, 1.18 mmol) and **compound 8** (1.61 g, 4.31 mmol) were dissolved in 25 mL of freshly distilled THF under an argon atmosphere. Before the addition of catalyst $PdCl_2(PPh_3)_2$ (75.55 mg, 0.11 mmol), the reaction medium was purged with argon for half an hour. Then, the reaction was stirred overnight at 80 ^oC. The solvent was removed under applying reduced pressure. In order to purify the crude product, column chromatography was used with hexane and chloroform (4:1). Thereafter the purification process, **compound 9** was obtained (0.49 g, 81%).

^{1}H NMR (400 MHz, $CDCl_3$) δ 8.11 (dd, J = 3.6, 0.9 Hz, 2H), 7.63 (s, 2H), 7.38 (dd, J = 5.1, 0.8 Hz, 2H), 7.18 (dd, J = 5.0, 3.7 Hz, 2H), 4.75 (d, J = 6.6 Hz, 2H), 2.35 – 2.30 (m, 1H), 1.36 – 1.25 (m, 32H), 0.89 – 0.87 (m, 6H). **^{13}C NMR** (100 MHz, $CDCl_3$) δ 141.86, 139.90, 127.96, 126.82, 125.38, 123.43, 122.51, 59.87, 38.97, 31.81, 31.32, 29.79, 29.54, 29.25, 26.15, 22.59, 14.04.

2.2.7. Synthesis of 4,7-bis(5-bromothiophen-2-yl)-2-(2-octyldodecyl)-2H-benzo [*d*][1,2,3]triazole(10)

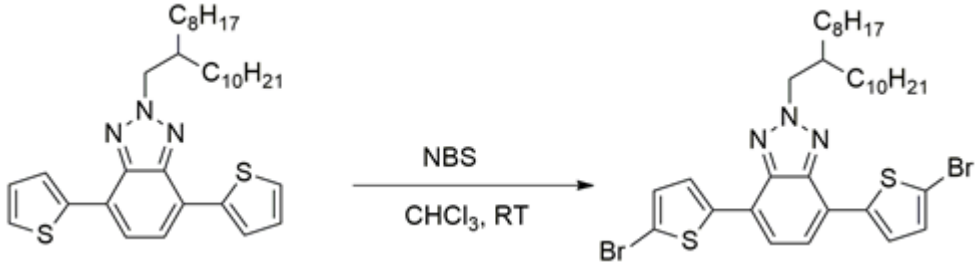

Figure 2.7. Synthesis of compound 10

N-bromosuccinimide (0.31 g, 1.76 mmol) was put portion by portion to the solution of **compound 9** (0.45 g, 0.80 mmol) in chloroform under dark conditions, following by stirring the reaction overnight under the same conditions. Extraction of the product was performed with DCM and distilled water. Further purification procedure was accomplished with the usage of column chromatography with hexane and chloroform (5:1). Desired yellow solid **compound 10** was obtained (0.49 g, 85%).

^{1}H NMR (400 MHz, $CDCl_3$) δ 7.78 (d, J = 3.9 Hz, 2H), 7.50 (s, 2H), 7.11 (d, J = 3.9 Hz, 2H), 4.72 (d, J = 6.6 Hz, 2H), 2.29 (m, 1H), 1.40 – 1.23 (m, 32H), 0.91 – 0.84 (m, 6H). **^{13}C NMR** (100 MHz, $CDCl_3$) δ 141.59, 141.28, 130.85, 126.86, 122.94, 122.06, 113.20, 59.99, 39.12, 31.96, 31.92, 31.44, 29.93, 29.68, 29.62, 29.39, 29.36, 26.27, 22.73, 14.18.

2.2.8. Synthesis of tributyl(selenophen-2-yl)stannane(12)

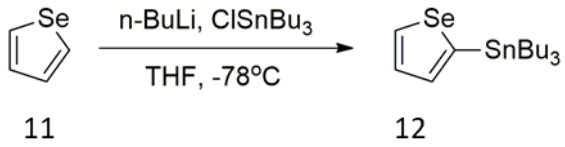

Figure 2.8. Synthesis of compound 12

After dissolving **Compound 11** (1.70 g, 12.97 mmol) in 20 mL of distilled THF, the reaction temperature was reduced to -78 ℃. The solution of n-BuLi (0.79 g, 2.5 M in hexane, 12.32 mmol) was introduced to the reaction medium drop by drop. After that, the reaction mixture was allowed to be stirred at -78 ℃ for one hour. The addition of tributyltin chloride (4.65 g, 14.27 mmol) into the reaction mixture dropwise at the same temperature was accomplished before stirring an additional one more hour at -78 ℃. The reaction mixture was warmed up to room temperature and was stirred overnight. The mixture was extracted with water and chloroform and dried over $MgSO_4$. There was no further purification step. Chloroform was evaporated with the rotary evaporator to obtain **compound 12** as the desired product (4.55 g, 83%).

2.2.9. Synthesis of 2-(2-octyldodecyl)-4,7-di(selenophen-2-yl)-2H-benzo[*d*] [1,2,3]triazole(13)

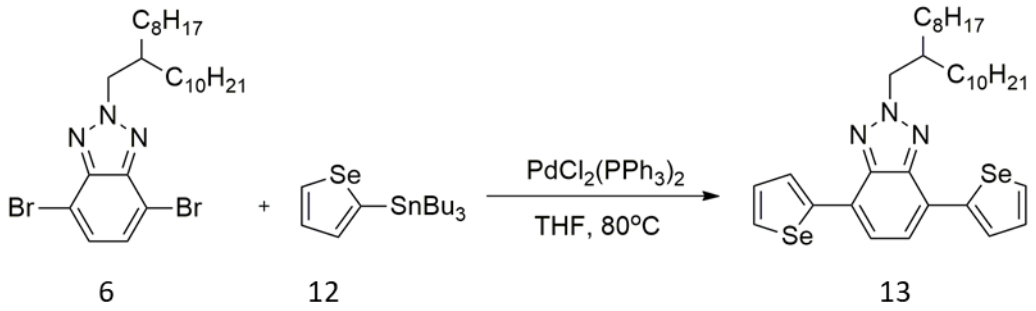

Figure 2.9. Synthesis of compound 13

Compound 6 (0.50 g, 0.90 mmol) and **compound 12** (1.13 g, 2.69 mmol) were dissolved in 20 mL of dry THF under an argon atmosphere before the addition of Pd catalyst (75.55 mg, 0.11 mmol), the reaction medium purged with argon for one hour. Then, the solution was stirred overnight at 80 °C. With the help of reduced pressure, solvent evaporation was performed. The purification of crude product was achieved by column chromatography via using hexane-chloroform in 5 to 1 ratio to afford **compound 13** as a yellow solid (0.47 g, 80%).

^{1}H NMR (400 MHz, $CDCl_3$) δ 8.12 (dd, J = 3.9, 0.9 Hz, 2H), 8.01 (dd, J = 5.6, 0.9 Hz, 2H), 7.54 (s, 2H), 7.35 (dd, J = 5.6, 3.9 Hz,2H), 4.68 (d, J = 6.4 Hz, 2H), 2.26 – 2.19 (m, 1H), 1.33 – 1.16 (m, 32H), 0.82 – 0.78 (m, 6H). **^{13}C NMR** (100 MHz, $CDCl_3$) δ 143.74, 140.37, 130.00, 128.97, 126.60, 123.95, 121.35, 58.38, 37.69, 30.51, 30.48, 30.10, 28.48, 28.24, 28.19, 27.94, 24.93, 21.28, 12.72.

2.2.10. Synthesis of 4,7-bis(5-bromoselenophen-2-yl)-2-(2-octyldodecyl)-2H-benzo[*d*][1,2,3]triazole(14)

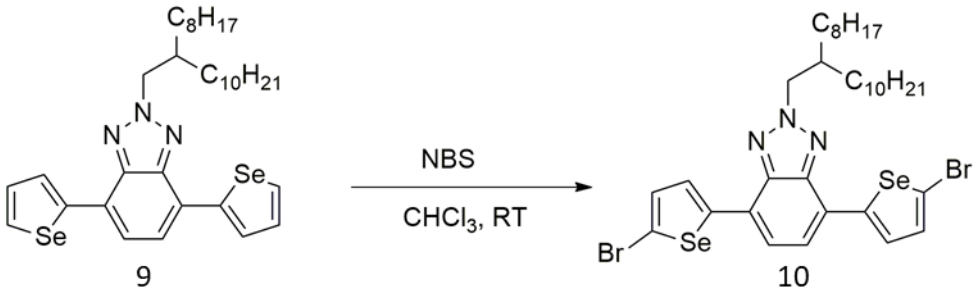

Figure 2.10. Synthesis of compound 14

Under dark conditions, a solution of **compound 13** (0.40 g, 0.60 mmol) was prepared with a sufficient amount of chloroform. Then, NBS (0.24 g, 1.34 mmol) was put in small amounts to the reaction mixture at ambient temperature, followed by stirring the reaction overnight with the same conditions. Extraction of the product was done with dichloromethane (DCM) and distilled water. After that, the column chromatography with hexane and chloroform (30:1) was achieved to obtain **compound 14** as a yellow solid (0.38 g, 77%).

^{1}H NMR (400 MHz, $CDCl_3$) δ 7.72 (d, J = 4.2 Hz, 2H), 7.48 (s, 2H), 7.26 (d, J = 4.2 Hz, 2H), 4.66 (d, J = 6.4 Hz, 2H), 2.19 (m, 1H), 1.35 – 1.10 (m, 32H), 0.86 – 0.72 (m, 6H). **^{13}C NMR** (100 MHz, $CDCl_3$) δ 146.30, 141.42, 133.44, 126.90, 124.62, 121.48, 117.64, 59.70, 39.05, 31.82, 31.39, 29.81, 29.59, 29.26, 26.23, 22.59, 14.04.

2.2.11. Synthesis of 4-bromo-1-((2-ethylhexyl)oxy)-2-fluorobenzene(15)

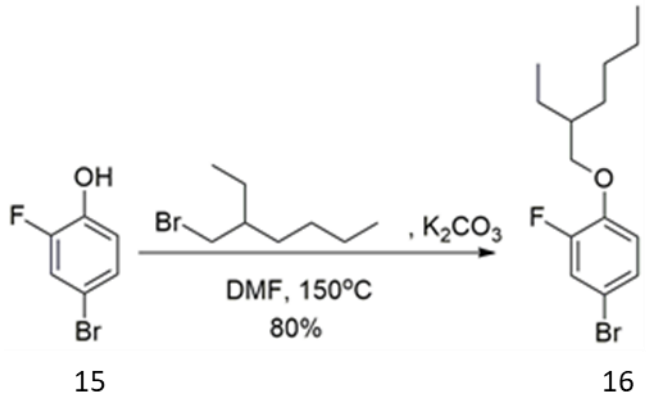

Figure 2.11. Synthesis of compound 15

Compound 15 (5.00 g, 26.18 mmol) and K_2CO_3 (4.34 g, 31.41 mmol) were dissolved in 50 mL of anhydrous DMF under an inert atmosphere. The mixture was purged with argon for 30 minutes at 65 °C before addition 3-(bromomethyl)heptane (5.06 g, 26.18 mmol). After the addition of the brominated alkyl chain, the temperature of the reaction was allowed to reach 150 °C. The reaction medium was stirred for 10 hours at that temperature. After the temperature of the crude product was decreased to ambient temperature, the reaction solution was poured into 150 mL cold water. The mixture was extracted five times with chloroform; then, the water-insoluble organic layer was dried over $MgSO_4$ and evaporated under vacuum. In order to obtain **compound 16**, the purification process was done by silica gel column chromatography with petroleum ether (6.38 g, 80%).

^{1}H NMR (400 MHz, $CDCl_3$) δ 7.22 (dd, J = 10.5, 2.3 Hz, 1H), 7.16 (dd, J = 8.7, 1.5 Hz, 1H), 6.83 (t, J = 8.7 Hz, 1H), 3.88 (d, J = 5.4 Hz, 2H), 1.81 – 1.71 (m, 1H), 1.54 – 1.31 (m, 8H), 0.92 (m, 6H). **^{13}C NMR** (100 MHz, $CDCl_3$) δ 152.67 (d, J = 250.9 Hz), 146.91 (d, J = 10.5 Hz), 127.11 (d, J = 4.1 Hz), 119.60 (d, J = 21.3 Hz), 115.92, 111.65 (d, J = 8.2 Hz).

2.2.12. Synthesis of 4,8-bis(4-(2-ethylhexyl)oxy)-3-fluorophenyl)benzo[1,2-b:4,5-b']dithiophene(18)

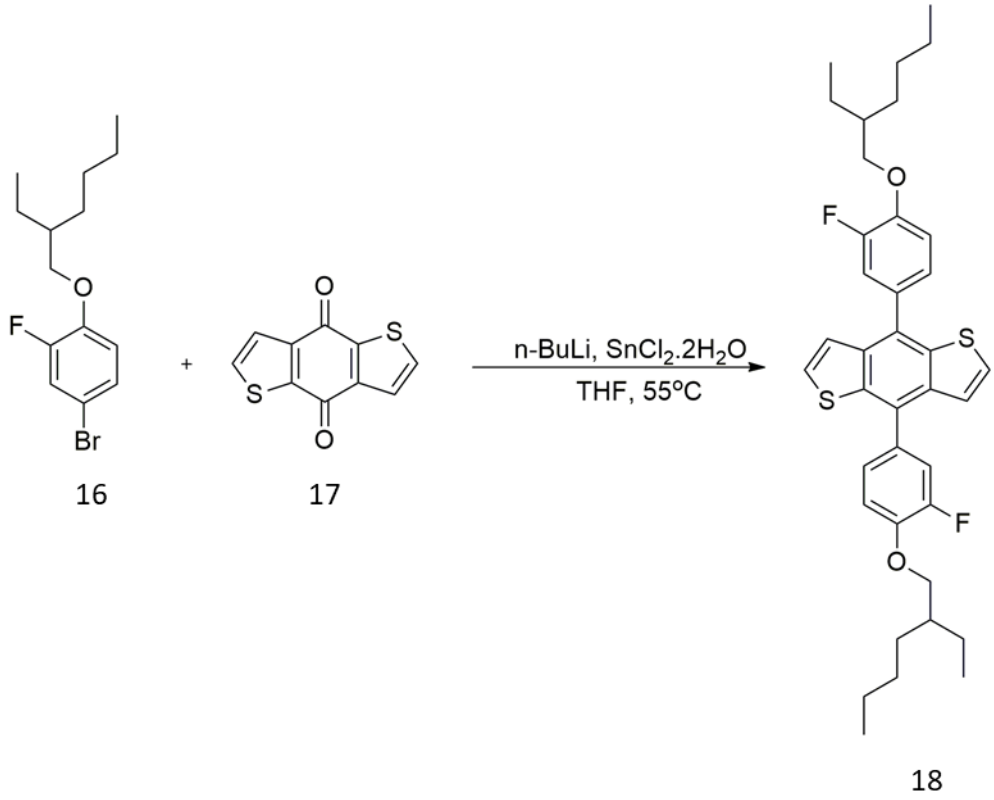

Figure 2.12. Synthesis of compound 18

Compound 16 (1.2 g, 3.96 mmol) was dissolved in 40 mL of dry THF. The reaction mixture purged with argon for one hour. Then the temperature of the mixture was decreased to -78 ℃, following by dropwise addition of n-BuLi (0.29 g, 2.5 M in hexane, 3.96 mmol). The temperature of the reaction was kept at -78 ℃ for 2 hours and **compound 17** (0.29 g, 1.32 mmol) was introduced into the solution. Then the temperature was raised to 55 ℃. After mixing the solution at that temperature for 2 hours, it was reduced to ambient temperature. Then, $SnCl_2.2H_2O$ (2.68 g, 11.87 mmol) in 10% HCl (15 mL) was added. The reaction medium was refluxed overnight. After that, it was poured into water and extracted with DCM. The

combined organic layers were washed with sodium bicarbonate and water solution several times and dried over $MgSO_4$. The solvent was evaporated under reduced pressure. Residual product was purified with silica gel column chromatography with hexane and chloroform (10:1). Further purification was done by recrystallization in hexane to obtain **compound 18** as yellow solid (0.57 g, 68%).

^{1}H NMR (400 MHz, $CDCl_3$) δ 7.45 – 7.39 (m, 6H), 7.33 (d, J = 5.7 Hz, 2H), 7.15 (t, J = 8.7 Hz, 2H), 4.03 (d, J = 6.0 Hz, 4H), 1.86 (m, 2H), 1.57 – 1.37 (m, 16H), 1.01 – 0.93 (m, 12H). **^{13}C NMR** (100 MHz, $CDCl_3$) δ 152.65 (d, J = 247.9 Hz), 147.42 (d, J = 10.9 Hz), 138.23 , 136.14, 131.70 (d, J = 6.6 Hz), 129.15, 127.48, 125.28 (d, J = 3.4 Hz), 122.83, 117.24 (d, J = 18.6 Hz), 114.76, 71.90, 39.44, 30.46, 29.10, 23.83, 23.10, 14.16, 11.16.

2.2.13. Synthesis of 4,8-bis(4-(2-ethylhexyl)oxy)-3-fluorophenyl)benzo[1,2-b:4,5-b']dithiophene-2,6-diyl)bis(trimethylstannane)(19)

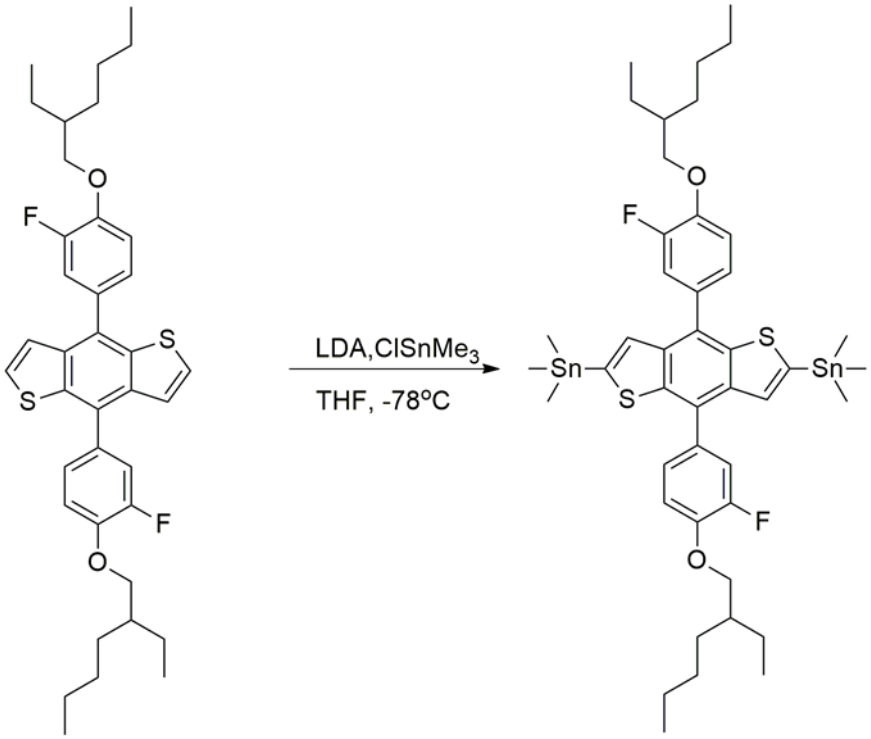

Figure 2.13. Synthesis of compound 19

A solution of **compound 18** (0.57 g, 0.90 mmol) was stirred in dry THF under an argon atmosphere. After the reaction medium was cooled to -78 ℃ with dry ice&acetone, LDA solution (0.29 g, 1.0 M in hexane, 2.69 mmol) was added dropwisely. The reaction was allowed to be stirred for 15 minutes at the same temperature, followed by the addition of trimethyltin chloride solution (0.51 g, 1.0 M in THF, 2.87 mmol) all at once. The reaction mixture was allowed to reach room temperature and stirred overnight. The extraction process was done with ether and water. The organic layer was dried over $MgSO_4$. To obtain the final product, the organic residue was purified by recrystallization technique in acetone (0.62 g, 72%).

^{1}H NMR (400 MHz, $CDCl_3$) δ 7.44 (dd, J = 15.5, 4.8 Hz, 4H), 7.35 (s, 2H), 7.16 (t, J = 8.6 Hz, 2H), 4.04 (d, J = 5.4 Hz, 4H), 1.88 – 1.83 (m, 2H), 1.59 – 1.39 (m, 32H), 1.04 – 0.93 (m, 12H), 0.46 (t, 18H). **^{13}C NMR** (100 MHz, $CDCl_3$) δ 152.67 (d, J = 247.0 Hz), 147.23 (d, J = 10.8 Hz), 142.47 (d, J = 17.8 Hz), 137.00, 132.46 (d, J = 6.7 Hz), 130.46, 127.58, 125.34 (d, J = 3.2 Hz), 122.81, 117.35 (d, J = 18.5 Hz), 114.78, 71.93, 39.53, 30.52, 29.13, 23.89, 23.09, 14.12, 11.17, -8.33.

2.3. Synthesis of Polymers

2.3.1. Synthesis of P1

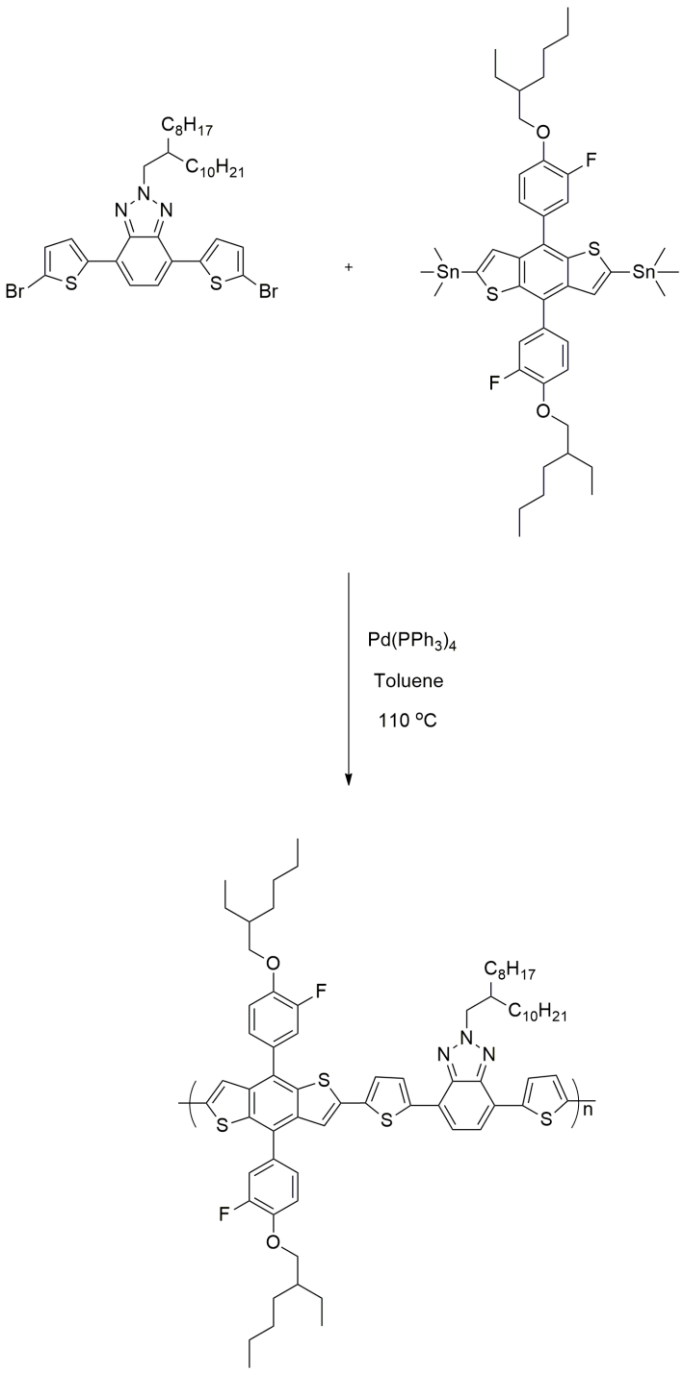

Figure 2.14. Synthesis of P1

Compound 19 (0.20 g, 0.2 mmol) and **compound 10** (0.15 g, 0.2 mmol) were dissolved in 15 mL dry toluene and purged with argon for one hour before addition of $Pd(PPh_3)_4$ (0.01 g, 0.01 mmol) catalyst. The reaction was refluxed for 30 hours at 110 ℃ under inert conditions. To complete polymerization, 2-bromothiophene (65.2 mg, 0.4 mmol) and 2-tributylstannylthiophene (149.2 mg, 0.4 mmol) were introduced into the reaction. After waiting an additional 3 hours, the toluene was reduced from the medium by using rotary evaporator. Ice-cold methanol poured into the polymer containing flask. Then, the product was filtered by a suction filter. Purification was done by Soxhlet extractor with methanol, acetone, hexane and chloroform, respectively. The polymer was recovered from $CHCl_3$ which was reduced from the medium with the help of a rotary evaporator later. After that, the residue was precipitated in cold methanol once more and filtered with vacuum to obtain P1 as a reddish-purple solid (0.21 g, 82%).

GPC results: M_n: 10 kDa, M_w: 42 kDa, PDI: 4.22

2.3.2. Synthesis of P2

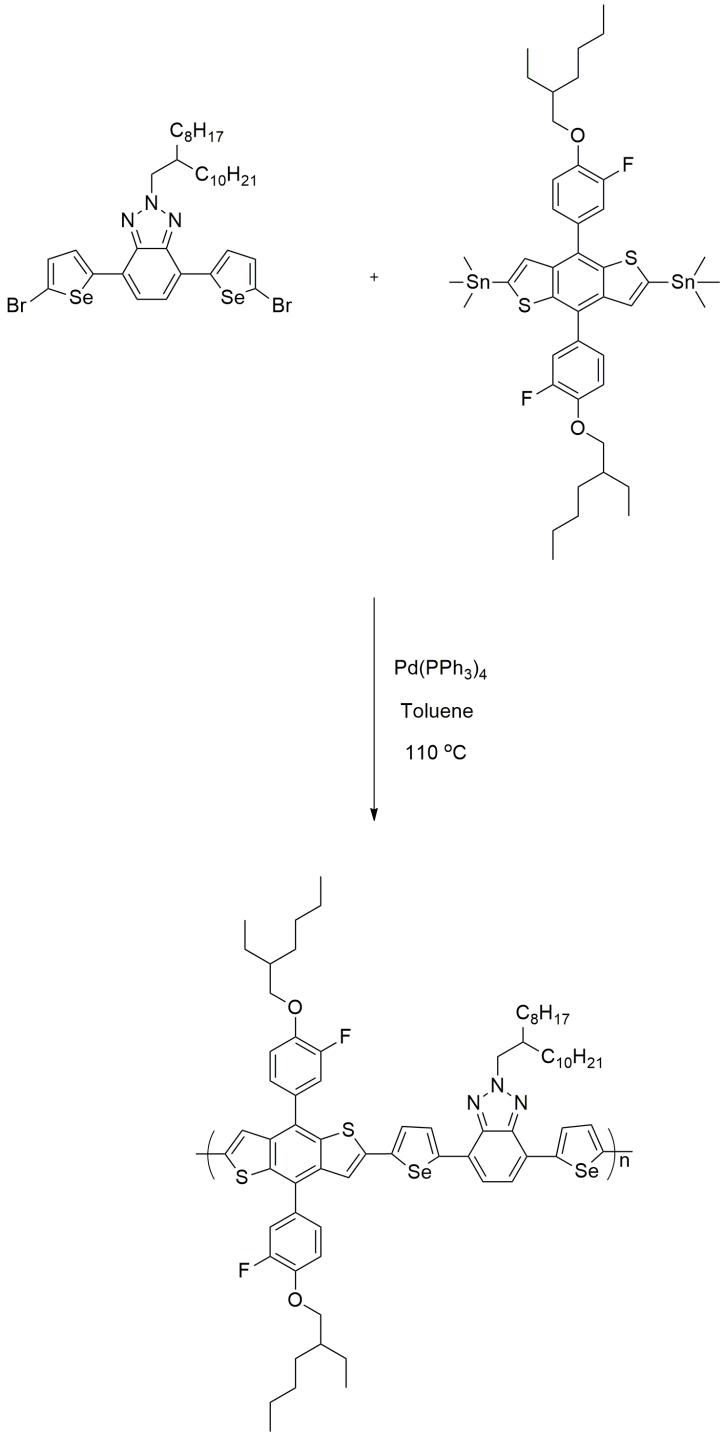

Figure 2.15. Synthesis of P2

Compound 19 (0.19 g, 0.2 mmol) and **compound 14** (0.17 g, 0.2 mmol) were dissolved in 15 mL dry toluene and purged with argon for one hour before addition of $Pd(PPh_3)_4$ (0.01 g, 0.01 mmol) catalyst. The reaction was refluxed for 30 hours at 110 ℃ under an argon atmosphere. To finalize polymerization, at first, 2-bromothiophene (65.2 mg, 0.4 mmol) was added and 3 hours later, 2-tributylstannylthiophene (149.2 mg, 0.4 mmol) were introduced into the reaction. Ice-cold methanol was poured into the polymer containing flask and filtered. Purification was done by Soxhlet extractor with methanol, acetone, hexane and chloroform, respectively. The polymer was recovered from $CHCl_3$. Then, chloroform was reduced from the medium with a rotary evaporator. Precipitation was performed in cold methanol once more and filtered with vacuum. P2 was obtained as a blue-purple solid. (0.22 g, 82%).

GPC results: M_n: 15 kDa, M_w: 75 kDa, PDI: 4.99

2.4. Characterization of Conducting Polymers

2.4.1. Gel Permeation Chromatography

The gel permeation chromatography (GPC) is a simple and fast technique that utilized in the determination of the weight average (M_w) and the number average molecular weights (M_n), polydispersity index (PDI) of the synthesized polymers in a THF solution. For calibration of the chromatogram, polystyrene (PS) standards were used.

2.4.2. Electrochemical Studies

Cyclic voltammetry (CV) is a widespread method to examine not only the behaviors of polymers under oxidation/reduction reactions but also calculate their HOMO-

LUMO energy levels. Therefore, electronic band gap (E_g^{el}) of polymers could be determined. In this study, CV was utilized for investigating electrochemical properties of both P1 and P2. To perform the cyclic voltammetry studies, potentiostat with three electrode system where consisting of platinum (Pt) (counter electrode), silver (Ag) wire (reference electrode) and polymer coated ITO (working electrode) was used. In addition, Gamry Instrument Reference 600 Potentiostat was utilized to record oxidation/ reduction reactions.

2.4.3. Spectroelectrochemical Studies

In this study, spectroelectrochemical studies were conducted to gain better understanding how electrochromic features of polymers change under doping process. These studies were performed by using three electrode system which is in electrochemical cell. To conduct the studies, ITO coated glass substrate was coated by synthesized polymers that dissolved in chloroform. Generated polymer films on ITO were immersed in 0.1 M $TBAPF_6$/ACN. The UV-Vis-NIR absorption spectrum of polymers exhibits not only absorption features of polymers when they are at neutral states but also polaron and bipolaron characteristics. Moreover, change in colors of polymers under electrochemical reactions was demonstrated by UV-Vis-NIR absorption spectrum. By using the onset point of maximum absorption which could be measured from UV-Vis-NIR, the optical band gaps of P1 and P2 were calculated by the following formula;

$$E_g^{op} = \frac{1241}{\lambda_{max}^{onset}}$$

2.4.4. Kinetic Studies

Kinetic studies were determined optical contrast and the switching time values of the synthesized polymers between their redox states through the application of potential at certain wavelengths. Chronoamperometry were carried out to evaluate switching times of polymers as a function of transmittance change (ΔT%) and time. In addition, UV-Vis-NIR spectrophotometer was employed to monitor the change in optical transmittance of polymers by applying voltage and calculate their optical contrast values.

2.4.5. Thermal Studies

In this study, thermogravimetry analysis (TGA) and differential scanning calorimetry (DSC) were performed to gain better information about thermal properties of polymers. The change in polymer weight under certain atmosphere at controlled temperature was examined by thermogravimetry analysis. Besides, physical feature changes of polymers that take place via temperature against time were recorded by differential scanning calorimetry studies.

2.4.6. Photovoltaic Studies

To investigate the photovoltaic parameters of polymers, bulk heterojunction (BHJ) solar cell devices were constructed with ITO/PEDOT:PSS/Polymer:$PC_{71}BM$/LiF/Al architecture. In order to fabricate the devices, ITO coated glass substrate was initially etched with hydrochloric acid and cleaned with toluene, detergent, water, acetone and isopropyl alcohol in an ultrasonic bath. Further purification of ITO glass substrate was achieved by oxygen plasma treatment via Harrick Plasma Cleaner. The oxygen plasma treatment was crucial for the removal of organic impurities. Then, this step is followed by the spin coating of PEDOT:PSS at varied rpm values. For evaporation of water residues, the hot plate was utilized for 15 minutes. Polymer and

$PC_{71}BM$ blends with various blend concentrations and weight ratios were prepared, filtered and spin-coated onto the surface in a glove box under an inert atmosphere. The thermal deposition of LiF and Al was achieved by a vacuum evaporation chamber. To investigate current density- voltage (J-V) characteristics of synthesized polymers, Keithley 2400 source meter was utilized under AM1.5 G illumination.

CHAPTER 3

RESULT AND DISCUSSIONS

3.1. Electrochemical Studies

Cyclic voltammetry was operated to detect HOMO-LUMO levels of the polymers and also their band gaps. Three electrode system with platinum wire, silver wire and polymer coated ITO as counter electrode, reference electrode and working electrode, sequentially, was utilized to examine the reduction and oxidation potentials of synthesized polymers. After the spray coating of the polymers onto ITO coated glasses, working electrodes were prepared by immersing in 0.1 M $TBAPF_6$/ACN electrolyte solution. CV measurements were recorded with a scan rate of 100 mV/s. The n-dopable and p-dopable characteristic features of polymers which shows ambipolar feature can be seen in Figure 3.1.

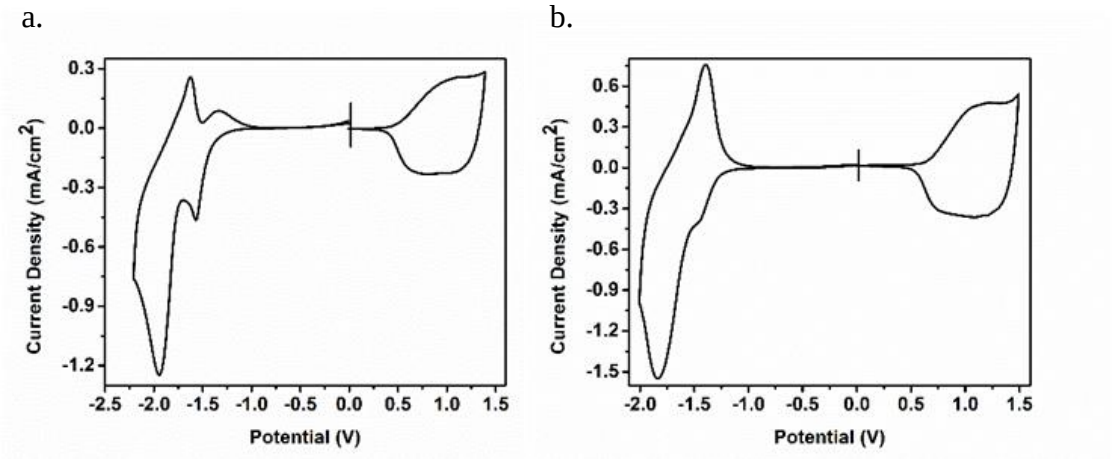

Figure 3.1. Cyclic voltammograms of polymers a) P1 b) P2 in 0.1 M $TBAPF_6$/ ACN electrolyte solution at a scan rate 100 mV/s

The p-type doping potentials of P1 and P2 were found as 0.92 V/ 1.10 V and 1.07 V/ 1.21 V. Also, the n-type doping potentials of P1 and P2 were evaluated as -1.57 V/ -1.95 V and -1.45 V/ -1.83 V. Since both polymers have n-dopable and p-dopable features, their HOMO and LUMO energy levels and band gaps were calculated from the following equations via using their onset potentials of oxidation and reduction.

$$HOMO = -(4.75 + E_{ox}^{onset})$$

$$LUMO = -(4.75 + E_{red}^{onset})$$

$$E_g^{el} = HOMO - LUMO$$

HOMO and LUMO energy levels of P1 were recorded as -5.25 eV and -3.34 eV, respectively, whereas HOMO and LUMO energy levels of P2 were recorded as -5.38 eV and -3.48 eV, respectively. The electronic band gap (E_g^{el}) values of P1 and P2 were detected as 1.91 eV and 1.90 eV, sequentially. Summary of electrochemical properties of P1 and P2 were demonstrated in Table 3.1. The synthesized polymers differ in their π-bridges which have different chalcogens in their structure. Selenophene based P2 has deeper LUMO than thiophene containing P1. The deeper LUMO energy level can be attributed to the higher polarizability of the selenium atom [57], [58].

Table 3.1. Summary of electrochemical studies of P1 and P2

	$E_{p\text{-doping}}$ (V)	$E_p^{onset}{}_{doping}$ (V)	$E_{n\text{-doping}}$ (V)	$E_n^{onset}{}_{doping}$ (V)	HOMO (eV)	LUMO (eV)	E_g^{el} (eV)
P1	0.92/ 1.10	0.50	-1.57/ -1.95	-1.41	-5.25	-3.34	1.91
P2	1.07/ 1.21	0.63	-1.45/ -1.83	-1.27	-5.38	-3.48	1.90

3.2. Spectroelectrochemical Studies

Light absorption behaviors of synthesized polymers with increasing applied potentials were examined. Three electrode system was used in the measurements of spectroelectrochemical characterization of polymers. By following the dissolution of the polymers in $CHCl_3$, they were transferred by spray coating to the surface of ITO coated glass. After immersing the ITO coated substrate in an electrolyte solution of 0.1 M $TBAPF_6$/ ACN in quartz cuvette, the absorption of polymers was recorded in the UV-vis-NIR range. Figure 3.2 exhibited the maximum absorption at 545 nm for P1 and 564 nm for P2, which points to π-π^* transitions between HOMO and LUMO energy levels of synthesized polymers [59]. Also, observed relative red shift in absorption maxima of selenophene containing P2 could be correlated with stronger interaction of polymer chain [60]. Summary of spectroelectrochemical studies of P1 and P2 were demonstrated in Table 3.2. The optical band gaps were determined from the onset points of maximum absorption wavelengths as 1.83 eV for P1 and 1.81 eV for P2.

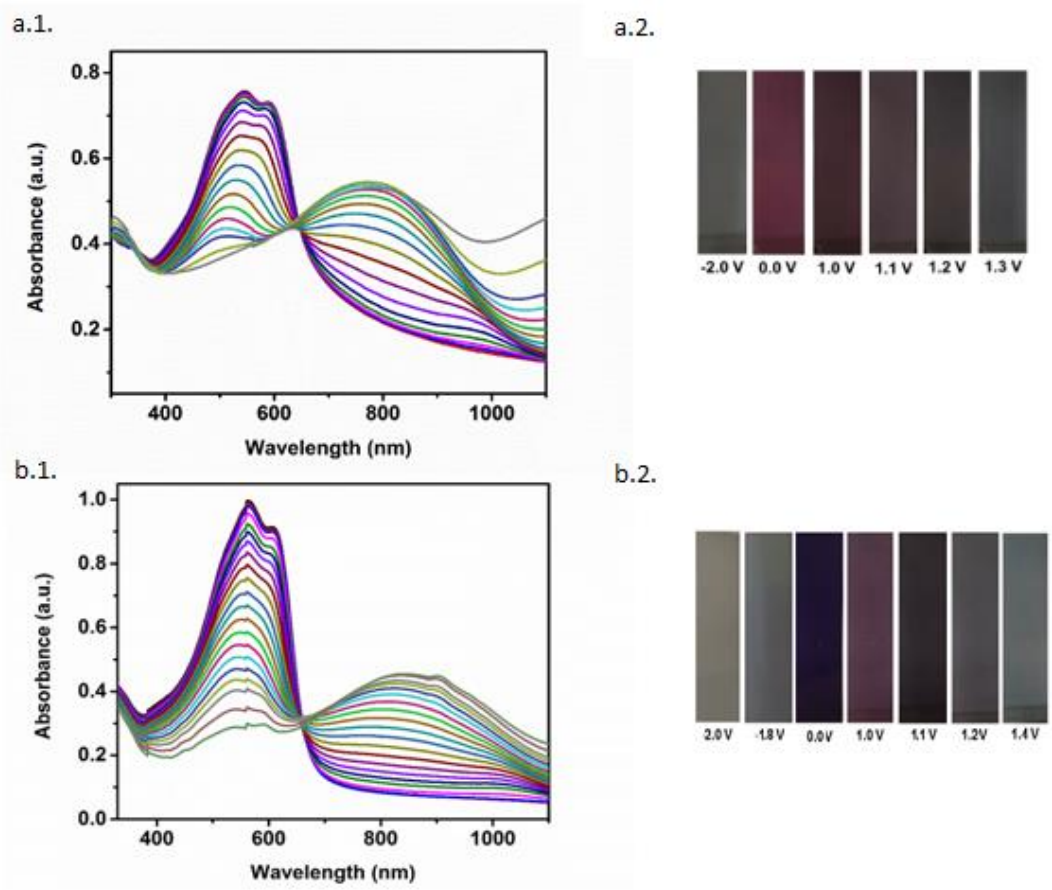

Figure 3.2 UV-Vis-NIR absorption spectra of a.1) P1 and b.1) P2 in 0.1 M $TBAPF_6$/ ACN electrolyte solution and the colors of a.2) P1 and b.2) P2 in the neutral, reduced and oxidized forms

Table 3.2. Summary of spectroelectrochemical studies of P1 and P2

Polymer	λ_{max} (nm)	λ_{max}^{onset} (nm)	E_g^{op} (eV)
P1	545/593	676	1.83
P2	564/609	685	1.81

3.3. Optical and Kinetic Studies

UV-Vis absorption spectra of P1 and P2 in thin film and solution were displayed in Figure 3.3 and summary of optical properties of P1 and P2 were demonstrated in Table 3.3. The broad absorption was accomplished as shown in the below figures. Both synthesized polymers showed two absorption peaks which originated from π-π* transitions and intermolecular charge transfer (ICT) between donor and acceptor units in the polymer backbones [61]. Different values of maximum absorption were obtained for solution and solid state of synthesized polymers which are 529 nm and 545 nm for P1 and 556 nm and 564 nm for P2, sequentially. Red-shifted absorption maxima and expansion through the longer wavelengths can be explained by aggregation in thin films [59], [62]. In addition, high polarization of selenium might be the reason behind obtaining absorption maxima at a longer wavelength for P2 [60].

Table 3.3. Summary of optical properties of P1 and P2

	Solution λ_{max} (nm)	Thin film λ_{max} (nm)
P1	510/ 529	545/ 593
P2	556/ 595	564/ 609

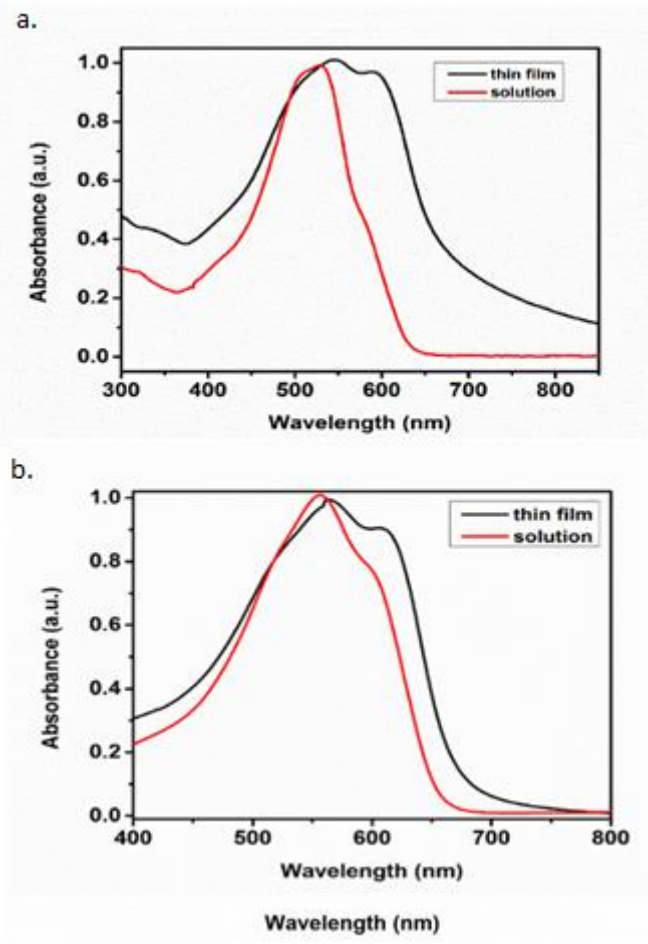

Figure 3.3. UV-Vis spectra of a) P1 and b) P2 in a chloroform solution and in the thin-film state

Kinetic studies of polymers were examined to declare optical contrast values and switching times by square wave voltammetry. Transmittance changes versus time graph of P1 and P2 were displayed in Figure 3.4 and Figure 3.5, sequentially. Also summary of kinetic studies of P1 and P2 were illustrated in Table 3.4.

.

a. b.

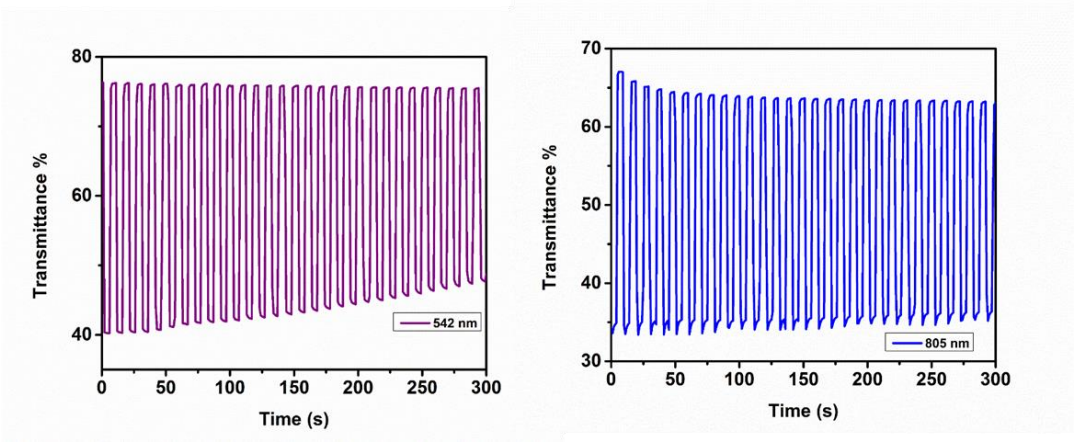

Figure 3.4. Percent transmittance changes of P1 at a) 542 nm b) 805 nm

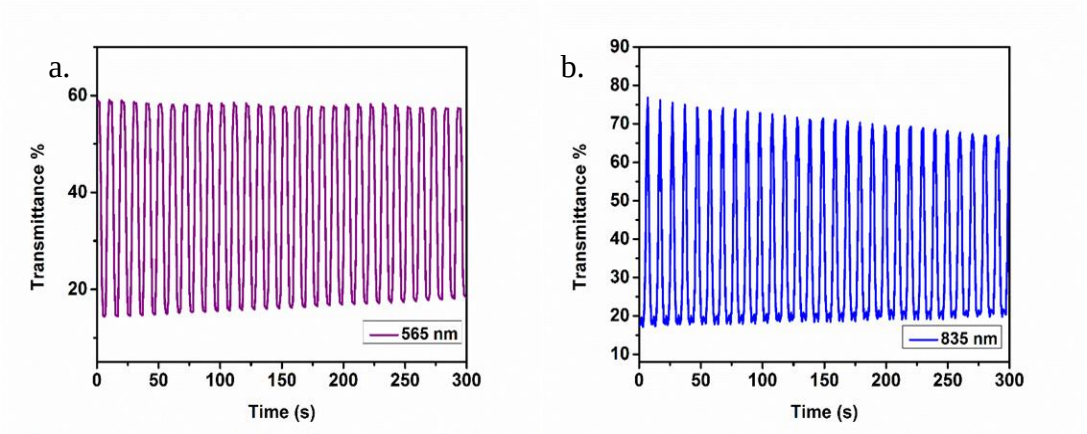

Figure 3.5. Percent transmittance changes of P2 at a) 565 nm b) 835 nm

In kinetic studies, the percent transmittance changes of P1 were reported as 37% at 542 nm and 31% at 805 nm with 1.2 s and 1.9 s switching time, respectively while optical contrast values of P2 were reported as 45% at 565 nm with 2.6 s switching time and 59% at 835 nm with 2.9 s switching time.

Table 3.4. Summary of kinetic studies of P1 and P2

		Optical contrast (%)	Switching Time (s)
P1	542 nm	37	1.2
	805 nm	31	1.9
P2	565 nm	45	2.6
	835 nm	59	2.9

3.4. Thermal Studies

Thermogravimetry analysis (TGA) and differential scanning calorimetry (DSC) were achieved to explore the thermal properties of polymers. TGA results indicated 47% weight loss at 590 ℃ for P1 and 50% weight loss at 645 ℃ for P2. DSC results showed that there are no glass transitions temperature (T_g) for both polymers. DSC and TGA analysis graphs were shown in Appendix B.

3.5. Photovoltaic Studies

Electrochemical and spectroelectrochemical studies show that the HOMO and LUMO energy levels and band gaps of polymers are suitable for bulk heterojunction which was illustrated in Figure 3.6.

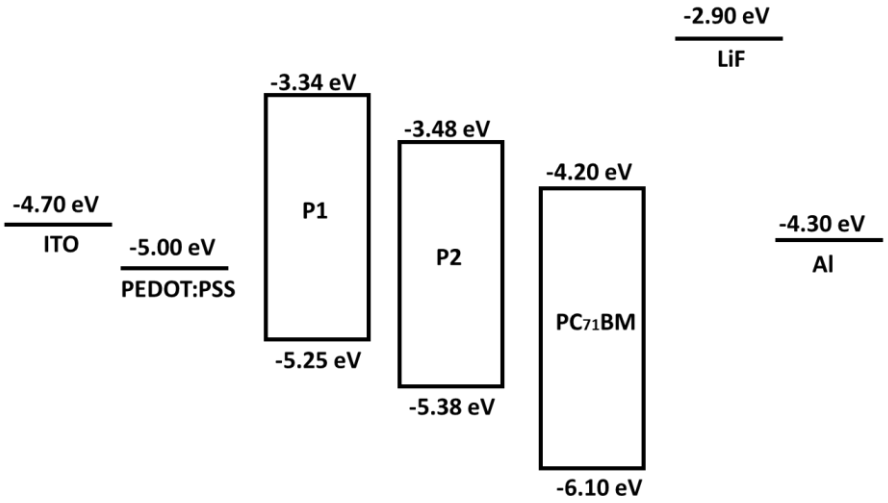

Figure 3.6. The energy levels of P1 and P2 used in bulk heterojunction device architecture

Bulk heterojunction BHJ solar cell devices were constructed with ITO/PEDOT:PSS/Polymer:$PC_{71}BM$/LiF/Al architecture and the parameters of constructed solar cells were investigated under air mass 1.5 G.

Different optimization techniques were performed, such as changing active layer thicknesses, blend concentration, Polymer:$PC_{71}BM$ ratio and using additives to increase power conversion efficiencies of devices.

The best power conversion result was reported as 1.40% for Polymer:$PC_{71}BM$ (1:3, w/w) with a J_{SC} 4.39 mA/cm^2, a V_{OC} of 0.71 V and a FF of 45% for P1. Additionally, for P2 PCE value obtained as 3.57% for Polymer:$PC_{71}BM$ (1:4, w/w) with a J_{SC} of 9.67 mA/cm^2 , a V_{OC} of 0.71 V ,and a FF of 52%.

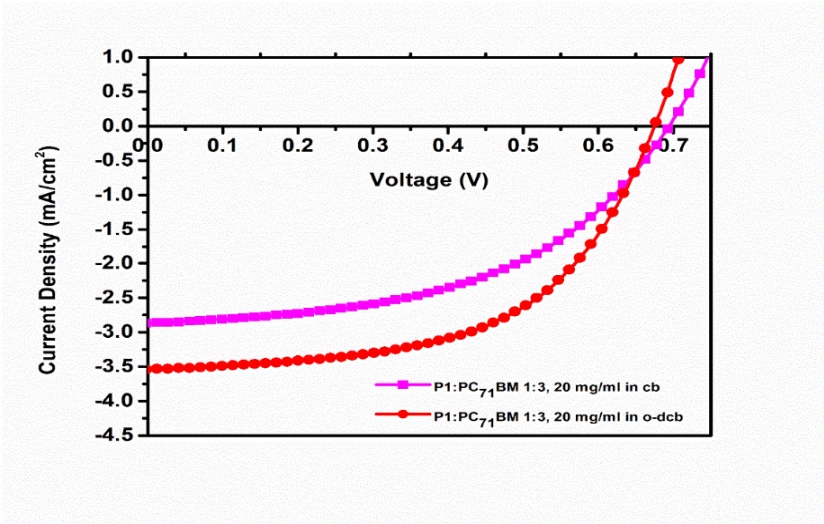

Figure 3.7. J−V curve of PSCs based on P1:$PC_{71}BM$ with different solvents

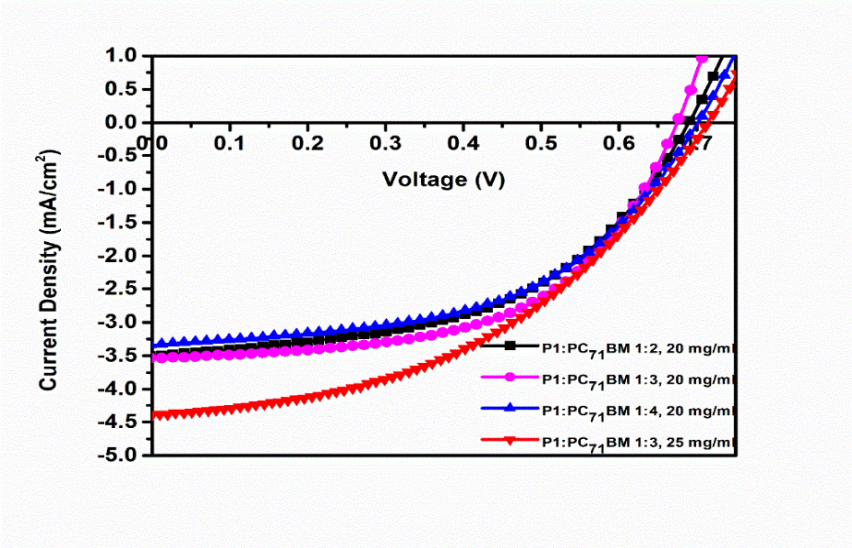

Figure 3.8. J-V curves that summarize photovoltaic performance of P1

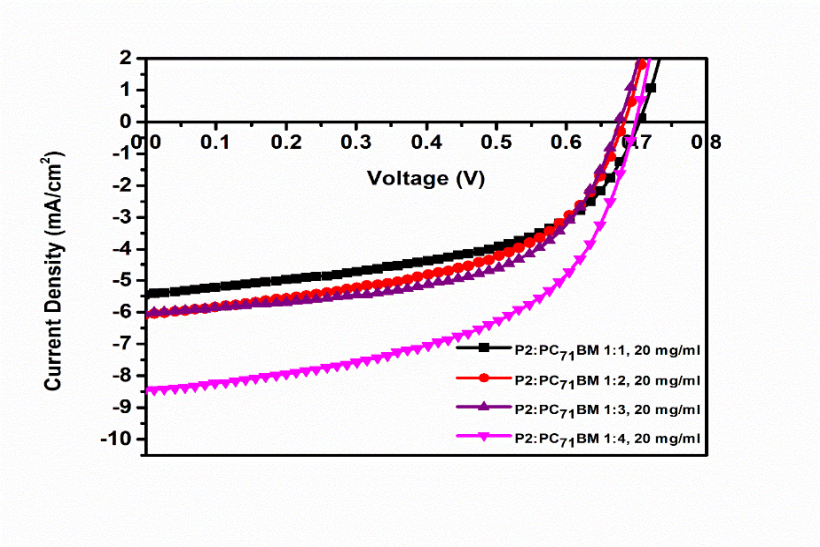

Figure 3.9. J−V curve of PSCs based on P2:PC_{71}BM with different D/A ratios

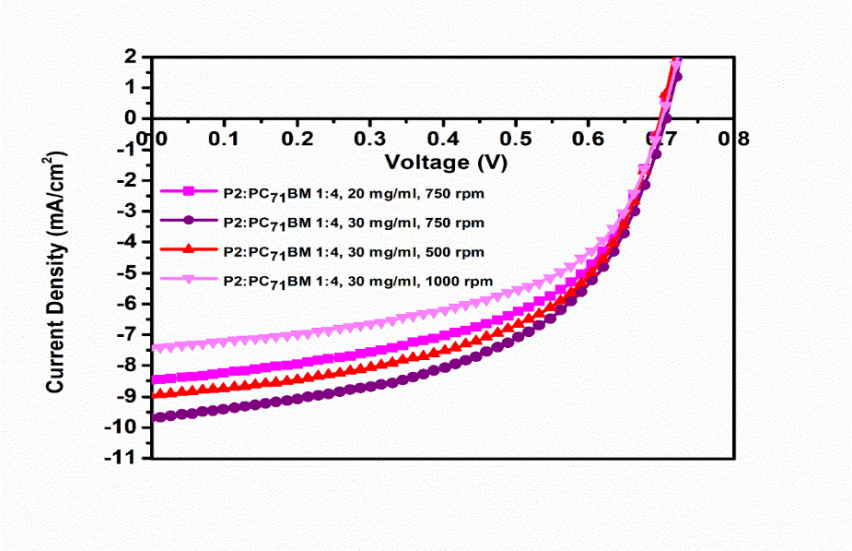

Figure 3.10. J−V curve of PSCs based on P2:PC_{71}BM with different spin coating rates

For the organic photovoltaic devices that comprise P1, the optimization procedure was tried with changing the Polymer:PC_{71}BM ratios and blend concentrations and spin coating rates. For the organic photovoltaic devices which contain P1, the

optimization procedures were tried with changing Polymer:$PC_{71}BM$ ratios and blend concentrations and spin coating rates. When Polymer:$PC_{71}BM$ ratio was increased 1:3 to 1:4, J_{SC} and power conversion efficiency of the device was decreased. In the active layer, polymer is responsible for absorbing incoming lights and the $PC_{71}BM$ has a role of charge transportation. The correlation between the two materials should be optimum due to these reasons. If the ratio of donor molecule $PC_{71}BM$ is higher than optimum, this can cause diminishment in light absorption, which reduces J_{sc} value and as a consequence, reduce the power conversion efficiency. When Polymer:$PC_{71}BM$ ratio was increased from 1:2 to 1:3, J_{SC} and power conversion efficiency of the device was increased. As mentioned before, optimum blend ratio is important for PCE of device; higher $PC_{71}BM$ in active layer blend increased the charge transportation. Moreover, 25 mg/mL blend concentration of Polymer:$PC_{71}BM$ (1:3, w/w) with 500 rpm spin rate have higher PCE value over 20 mg/ml blend concentration of Polymer:$PC_{71}BM$ (1:3, w/w) with 500 rpm spin rate. The higher blend concentration of Polymer:$PC_{71}BM$ led to tightly packed morphology between acceptor and donor material thus reduce the phase separation and increase the power conversion efficiency in photovoltaics. The spin rate determines the thickness of the active layer. The increment in thickness results in higher light absorption; however, a thicker active layer obtained by lowering the spin rate can cause recombination. The thickness optimization was determined by changing spin rates 500 rpm to 750 rpm at 20 mg/mL blend concentration of Polymer:$PC_{71}BM$ (1:2, w/w) and the study showed that with increasing spin rate, power conversion efficiency was reduced.

For P2 comprising solar cell devices, Polymer:$PC_{71}BM$ ratio was shifted 1:3 to 1:4, the J_{SC} and PCE values were significantly improved from 6.06 mA/cm^2, 2.32% to 8.45 mA/cm^2, 3.16%. As mentioned above, the reason for this improvement is higher $PC_{71}BM$ ratio in the active layer enhances charge transportation. 30 mg/mL blend concentration of Polymer:$PC_{71}BM$ (1:4, w/w) have higher PCE value over 20 mg/mL blend concentration of Polymer:$PC_{71}BM$ (1:4, w/w). However, when the blend concentration was increased to 35 mg/mL, the power conversion efficiency of

the device was dramatically decreased with 750 rpm spin rate. Furthermore, to obtain higher PCE, the thickness optimization was done by changing the spin coating rate for the active layer. The coating rate with 500, 750 and 1000 rpm was tried with 30 mg/mL blend concentration of Polymer:$PC_{71}BM$ (1:4, w/w) and PCE was changed between 3.37%, 3.57%, 2.83%, respectively. As noted, 500 rpm spin rate coated devices have lower PCE than 750 rpm spin rate coated solar cells due to the recombination process; however, at 1000 rpm thinner films of the active layer cause lower light absorption. The addition of 2% diiodooctane (DIO) reduced the efficiency, and this might be a consequence of the poor interactions between active layer and additive.

Table 3.5. Summary of photovoltaic studies of P1

P1:$PC_{71}BM$ (w:w)	Concentration (mg/mL)	J_{sc} (mA/cm^2)	V_{oc} (V)	FF (%)	RPM	PCE (%)
1:3 (CB)	20	2.86	0.69	50	500	0.99
1:3 (o-DCB)	20	3.54	0.67	56	500	1.32
1:2 (o-DCB)	20	3.49	0.69	51	500	1.22
1:2 (o-DCB)	20	2.52	0.69	54	750	0.94
1:4 (o-DCB)	20	3.35	0.70	51	500	1.21
1:3 (o-DCB)	**25**	**4.39**	**0.71**	**45**	**500**	**1.40**

Table 3.6. Summary of photovoltaic studies of P2

P2:$PC_{71}BM$ (w:w)	Concentration (mg/mL)	J_{sc} (mA/cm^2)	V_{oc} (V)	FF (%)	RPM	PCE (%)
1:1(o-DCB)	20	5.42	0.70	52	750	1.99
1:2(o-DCB)	20	6.08	0.68	51	750	2.13
1:3(o-DCB)	20	6.06	0.67	57	750	2.32
1:4(o-DCB)	20	8.45	0.70	53	750	3.16
1:4(o-DCB)	**30**	**9.67**	**0.71**	**52**	**750**	**3.57**
1:4(o-DCB)	35	4.87	0.68	28	750	0.92
1:4(o-DCB)	30	9.01	0.70	53	500	3.37
1:4(o-DCB)	30	7.45	0.70	54	1000	2.83
1:4(o-DCB)[a]	30	7.62	0.66	47	750	2.36

[a]The additive treatment with 2% DIO

The external quantum efficiencies of devices were quantified to examine the accuracy of photovoltaics. The highest EQE value was calculated as 18% for P1 and 45% for P2, respectively. External quantum efficiency curves for best performance photovoltaics of P1 and P2 were illustrated in Figure 3.11.

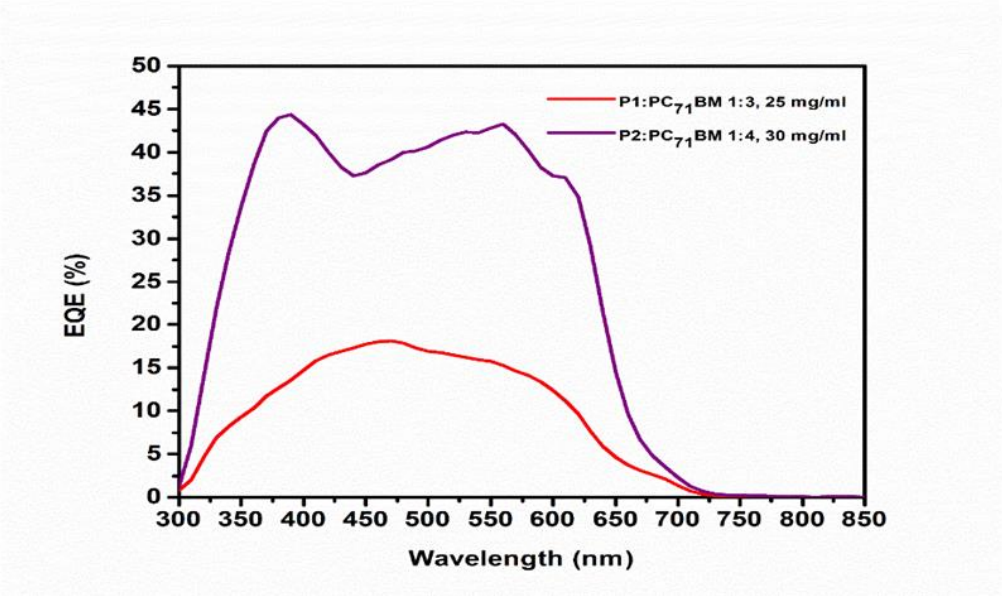

Figure 3.11. External quantum efficiency curves for best performance photovoltaics of P1 and P2

3.6. Morphology

The efficiency of a solar device is highly affected by the morphology of the active layer. The photoactive layer of best performance devices' morphologies were investigated via Atomic Force Microscopy (AFM). The efficiency of a solar device is highly affected by the morphology of the active layer. The photoactive layer of best-performance devices' morphologies was investigated via atomic Force Microscopy (AFM) and transmission electron microscopy (TEM). The thicknesses and the surface roughnesses of the active layer were examined from AFM images shown in Figure 3.12. The thickness and the surface roughness of the active layer of P1 containing cell are 91 nm and 0.827 nm. Moreover, P2 containing active layer has 98 nm active layer thickness with 1.71 nm surface roughness. In literature, optimum active layer thickness for bulk heterojunction solar cells is reported as around 80-100 nm; thus, both devices are compatible with the literature [63].

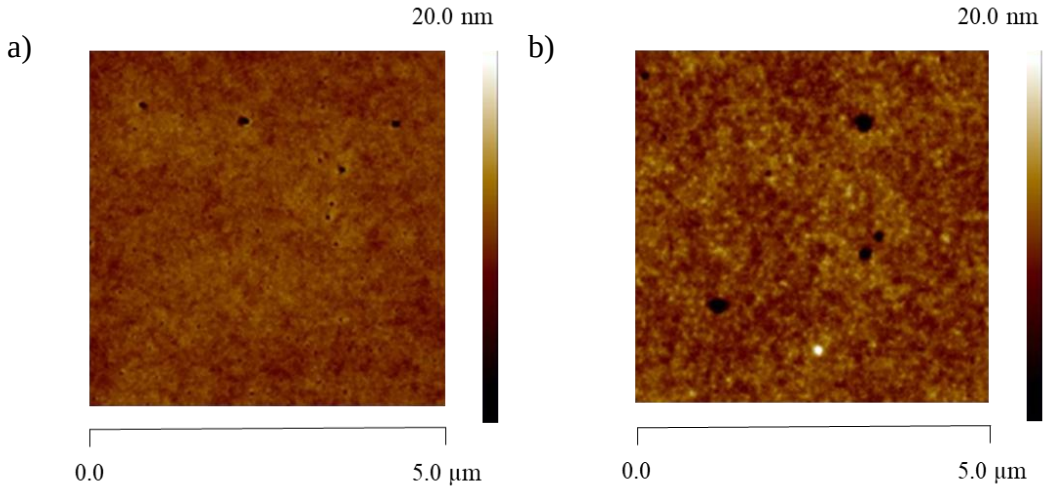

Figure 3.12. AFM images of a) P1:$PC_{71}BM$ (1:3, w/w) with 25 mg/mL blend concentration b) P2:$PC_{71}BM$ (1:4, w/w) with 30 mg/mL blend concentration

In the Figure 3.13, the TEM images were depicted. Dark grey spots are $PC_{71}BM$ and the lighter spots are polymers in the blend. Both best-performanced devices were shown homogenous mixture; however, the second device that contains P2 has undissolved $PC_{71}BM$ (black spots) and aggregation. The more interpenetrated donor-acceptor blends in P2: $PC_{71}BM$ containing device might overcame the problems that aggregation caused since fill factor of P2 comprised cell is higher than P1 containing device. Moreover, the more narrow fibril formation of P2 containing cell might be led to enhanced exciton dissociation and higher J_{sc} values that are coherent with the solar cells' photovoltaic results.

a) b)

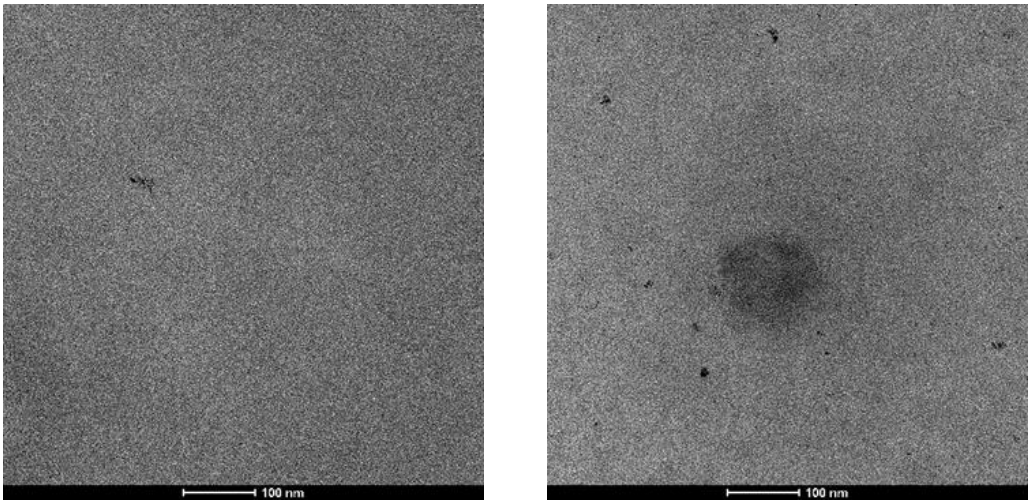

Figure 3.13. TEM images of a) P1:$PC_{71}BM$ (1:3, w/w) with 25 mg/mL blend concentration b) P2:$PC_{71}BM$ (1:4, w/w) with 30 mg/mL blend concentration

CHAPTER 4

CONCLUSION

In this study, benzodithiophene and benzotriazole containing two new donor-acceptor type alternating copolymer with two different π bridges were synthesized via Stille cross-coupling reaction. Synthesized compounds' structures were affirmed with ^{1}H and ^{13}C nuclear magnetic resonance spectroscopy. Both polymers did not suffer from low solubility due to long branched alkyl chains on acceptor and donor units of P1 and P2. The number average molecular weights of P1 and P2 were reported as 10 kDa and 15 kDa by GPC. Electrochemical, optical, spectroelectrochemical and kinetic studies of P1 and P2 were examined to determine their suitability for photovoltaic application. Both polymers exhibit a broad absorption range in UV-Vis-NIR spectra with the maximum absorptions 545 nm and 564 nm for P1 and P2, sequentially. The optical band gaps were evaluated from the onset points of maximum absorption wavelengths and the values were found as 1.83 eV and 1.81 eV for P1 and P2, correspondingly. From cyclic voltammetry, HOMO and LUMO energy levels of P1 were recorded as -5.25 eV/ -3.34 eV, whereas HOMO and LUMO energy levels of P2 were recorded as -5.38 eV/-3.48 eV, sequentially. Both polymers showed ambipolar character and the band gap (E_g^{el}) values of P1 and P2 were calculated as 1.91 eV and 1.90 eV. In their neutral states, P1 had red-purple color while P2 had blue-purple color in thin films of polymers. In kinetic studies, the percent transmittance changes were reported as 37% at 542 nm and 31% at 805 nm with 1.2 s and 1.9 s switching time, respectively for P1 and while optical contrast values of P2 were reported as 45% at 565 nm with 2.6 s switching time and 59% at 835 nm with 2.9 s switching time. The best power conversion result was reported as 1.40% for Polymer:$PC_{71}BM$ (1:3, w/w) with a J_{SC} of 4.39 mA/cm^2, a V_{OC} of 0.71 V and a FF of 45% for P1. Additionally, for P2 PCE value obtained as 3.57% for Polymer:$PC_{71}BM$ (1:4, w/w) with a J_{SC} of 9.67 mA/cm^2, a V_{OC} of 0.71 V

and a FF of 52% with ITO/PEDOT:PSS/Polymer:$PC_{71}BM$/LiF/Al bulk heterojunction solar device construction. In this work, the effects of different π-conjugated linkers were investigated. Selenophene has more quinoidal and electron rich character than thiophene, so P2 was expected to have a lower band gap. However, changing π-spacers did not have a significant influence on the band gap and absorption spectra. In the photovoltaic studies, selenophene bearing P2 has shown higher J_{SC} and hence higher PCE values might be resulted from higher hole mobility. Moreover, meta-fluorinated alkoxy phenyl side chain has been employed as an alternative to alkoxy group on BDT structure. The study was showed using m-F-benzodithiophene was provided lower HOMO energy level and higher V_{OC} values for P2 than literature analog P-SBTBDT since the V_{OC} is directly dependent on the energy difference between HOMO energy level of donor material (polymer) and LUMO energy level of acceptor material ($PC_{71}BM$). The results indicate using fluorinated side chain in the polymers and using selenophene as a π-bridge is a promising method to enhance V_{OC}, J_{SC} and improve power conversion efficiency.

REFERENCES

[1] H. Shirakawa, E. J. Louis, A. G. MacDiarmid, C. K. Chiang, and A. J. Heeger, "Synthesis of electrically conducting organic polymers: Halogen derivatives of polyacetylene, (CH)x," *J. Chem. Soc. Chem. Commun.*, no. 16, pp. 578–580, 1977.

[2] N. Basescu, Z.-X. Liu, D. Moses, A. J. Heeger, H. Naarmann, and N. Theophilou, "High electrical conductivity in doped polyacetylene," *Nature*, vol. 327, no. 6121, pp. 403–405, 1987.

[3] J. D. Stenger-Smith, "Intrinsically electrically conducting polymers. Synthesis, characterization, and their applications," *Prog. Polym. Sci.*, vol. 23, no. 1, pp. 57–79, 1998.

[4] O. Ostroverkhova, "Organic Optoelectronic Materials: Mechanisms and Applications," *Chem. Rev.*, vol. 116, no. 22, pp. 13279–13412, 2016.

[5] A. G. MacDiarmid, ""Synthetic Metals": A Novel Role for Organic Polymers (Nobel Lecture).," *Angew. Chemie Int. Ed.*, vol. 40, no. 14, pp. 2581–2590, 2001.

[6] A. K. Bakhshi and G. Bhalla, "Electrically conducting polymers: Materials of the twentyfirst century," *J. Sci. Ind. Res. (India).*, vol. 63, no. 9, pp. 715–728, 2004.

[7] I. Capek, *Radical Polymerisation Polyelectrolytes*. 1999.

[8] M. A. De Paoli and G. A, "Electrochemistry, polymers and opto-electronic devices: A combination with a future," *J. Braz. Chem. Soc.*, vol. 13, no. 4, pp. 12023–12030, 2002.

[9] J. Roncali, "Molecular Engineering of the Band Gap of π-Conjugated Systems: Facing Technological Applications," *Macromol. Rapid Commun.*, vol. 28, no. 17, pp. 1761–1775, 2007.

[10] J. Roncali, “Synthetic principles for bandgap control in linear π-conjugated systems,” *Chem. Rev.*, vol. 97, no. 1, pp. 173–205, 1997.

[11] E. E. Havinga and E. W. Meijer, “Developments in the chemistry and band gap engineering of donor - acceptor substituted conjugated polymers,” *Mater. Sci. Eng.*, vol. 32, no. 1, pp. 1–40, 2001.

[12] J. L. Brédas, “Relationship between band gap and bond length alternation in organic conjugated polymers Relationship between band gap and bond length alternation in organic conjugated polymers,” *J. Chem. Phys.*, vol. 82, no. 8, pp. 3808–3811, 1985.

[13] H. Brisset, P. Blanchard, B. Illien, A. Riou, and J. Roncali, “Bandgap control through reduction of bond length alternation in bridged poly(diethienylethylene)s,” *Chem. Commun.*, no. 6, pp. 569–570, 1997.

[14] C. Chochos and S. Choulis, “How the structural deviations on the backbone of conjugated polymers influence their optoelectronic properties and photovoltaic performance,” *Prog. Polym. Sci.*, vol. 36, no. 10, pp. 1326–1414, 2011.

[15] Y.-J. Cheng, S.-H. Yang, and C.-S. Hsu, “Synthesis of Conjugated Polymers for Organic Solar Cell Applications,” *Chem. Rev.*, vol. 109, no. 11, pp. 5868–5923, 2009.

[16] C. Liu, K. Wang, X. Gong, and A. J. Heeger, “Low bandgap semiconducting polymers for polymeric photovoltaics,” *Chem. Soc. Rev.*, vol. 45, no. 17, pp. 4825–4846, 2016.

[17] E. E. Havinga, W. ten Hoeve, and H. Wynberg, “Alternate donor-acceptor small-band-gap semiconducting polymers; Polysquaraines and polycroconaines,” *Synth. Met.*, vol. 55, no. 1, pp. 299–306, 1993.

[18] C. Kitamura, S. Tanaka, and Y. Yamashita, “Design of Narrow-Bandgap Polymers. Syntheses and Properties of Monomers and Polymers Containing

Aromatic-Donor and o-Quinoid-Acceptor Units," *Chem. Mater.*, vol. 8, no. 2, pp. 570–578, 1996.

[19] B. P. Rand *et al.*, "The Impact of Molecular Orientation on the Photovoltaic Properties of a Phthalocyanine / Fullerene Heterojunction," *Adv. Funct. Mater.*, vol. 22, no. 14, pp. 2987–2995, 2012.

[20] A. Tanimoto and T. Yamamoto, "Synthesis of n-Type Poly(benzotriazole)s Having p-Conducting and Polymerizable Carbazole Pendants," *Macromolecules*, vol. 39, no. 10, pp. 3546–3552, 2006.

[21] A. Balan, D. Baran, and L. Toppare, "Benzotriazole containing conjugated polymers for multipurpose organic electronic applications," *Polym. Chem.*, vol. 2, no. 5, pp. 1029–1043, 2011.

[22] D. B. Shaikh *et al.*, "Influences of Structural Modification of Naphthalenediimides with Benzothiazole on Organic Field-Effect Transistor and Non-Fullerene Perovskite Solar Cell Characteristics," *ACS Appl. Mater. Interfaces*, vol. 11, no. 47, pp. 44487–44500, 2019.

[23] H. Yao, L. Ye, H. Zhang, S. Li, S. Zhang, and J. Hou, "Molecular Design of Benzodithiophene-Based Organic Photovoltaic Materials," *Chem. Rev.*, vol. 116, 2016.

[24] B. Zheng, L. Huo, and Y. Li, "Benzodithiophenedione-based polymers: recent advances in organic photovoltaics," *NPG Asia Mater.*, vol. 12, no. 1, p. 3, 2020.

[25] G. Ö. Atlı, E. A. Yılmaz, S. T. Aslan, Y. A. Udum, L. Toppare, and A. Çırpan, "Synthesis and characterization of optical, electrochemical and photovoltaic properties of selenophene bearing benzodithiophene based alternating polymers," *J. Electroanal. Chem.*, vol. 862, p. 114014, 2020.

[26] H.-Y. Chen, S.-C. Yeh, C.-T. Chen, and C.-T. Chen, "Comparison of thiophene- and selenophene-bridged donor–acceptor low band-gap

copolymers used in bulk-heterojunction organic photovoltaics," *J. Mater. Chem.*, vol. 22, no. 40, pp. 21549–21559, 2012.

[27] H. Hoppe and N. S. Sariciftci, "Organic solar cells: An overview," *J. Mater. Res.*, vol. 19, no. 7, pp. 1924–1945, 2004.

[28] C. Lungenschmied *et al.*, "Flexible, long-lived, large-area, organic solar cells," *Sol. Energy Mater. Sol. Cells*, vol. 91, no. 5, pp. 379–384, 2007.

[29] D. Wöhrle and D. Meissner, "Organic Solar Cells," *Adv. Mater.*, vol. 3, no. 3, pp. 129–138, 1991.

[30] B. A. Gregg and M. C. Hanna, "Comparing organic to inorganic photovoltaic cells: Theory, experiment, and simulation," *J. Appl. Phys.*, vol. 93, no. 6, pp. 3605–3614, 2003.

[31] C. W. Tang, "Two-layer organic photovoltaic cell," *Appl. Phys. Lett.*, vol. 48, no. 2, pp. 183–185, 1986.

[32] G. Yu, J. Gao, J. C. Hummelen, F. Wudl, and A. J. Heeger, "Polymer Photovoltaic Cells: Enhanced Efficiencies via a Network of Internal Donor-Acceptor Heterojunctions," *Science.*, vol. 270, no. 5243, pp. 1789-1791, 1995.

[33] F. Yang, M. Shtein, and S. R. Forrest, "Controlled growth of a molecular bulk heterojunction photovoltaic cell," *Nat. Mater.*, vol. 4, no. 1, pp. 37–41, 2005.

[34] J. Nelson, "Polymer:fullerene bulk heterojunction solar cells," *Mater. Today*, vol. 14, no. 10, pp. 462–470, 2011.

[35] C. Deibel and V. Dyakonov, "Polymer-Fullerene Bulk Heterojunction Solar Cells," *Reports Prog. Phys.*, vol. 73, no. 9, pp. 1–39, 2010.

[36] Y. Huang, E. J. Kramer, A. J. Heeger, and G. C. Bazan, "Bulk Heterojunction Solar Cells: Morphology and Performance Relationships," *Chem. Rev.*, vol. 114, no. 14, pp. 7006–7043, 2014.

[37] M. C. Scharber and N. S. Sarciftci, "CHAPTER 2 Bulk Heterojunction

Organic Solar Cells: Working Principles and Power Conversion Efficiencies," in *Nanostructured Materials for Type III Photovoltaics*, The Royal Society of Chemistry, pp. 33–68, 2018.

[38] A. J. Heeger, "25th Anniversary Article: Bulk Heterojunction Solar Cells: Understanding the Mechanism of Operation," *Adv. Mater.*, vol. 26, no. 1, pp. 10–28, 2014.

[39] Y.-W. Su, S.-C. Lan, and K.-H. Wei, "Organic photovoltaics," *Mater. Today*, vol. 15, no. 12, pp. 554–562, 2012.

[40] J.-L. Brédas, J. E. Norton, J. Cornil, and V. Coropceanu, "Molecular Understanding of Organic Solar Cells: The Challenges," *Acc. Chem. Res.*, vol. 42, no. 11, pp. 1691–1699, 2009.

[41] P. Schilinsky, C. Waldauf, and C. J. Brabec, "Recombination and loss analysis in polythiophene based bulk heterojunction photodetectors," *Appl. Phys. Lett.*, vol. 81, no. 20, pp. 3885–3887, 2002.

[42] M.-E. Ragoussi and T. Torres, "New generation solar cells: concepts{,} trends and perspectives," *Chem. Commun.*, vol. 51, no. 19, pp. 3957–3972, 2015.

[43] H. A. McCartney and M. H. Unsworth, "Spectral distribution of solar radiation. I: Direct radiation," *Q. J. R. Meteorol. Soc.*, vol. 104, no. 441, pp. 699–718, 1978.

[44] S. R. Cowan, A. Roy, and A. J. Heeger, "Recombination in polymer-fullerene bulk heterojunction solar cells," *Phys. Rev. B*, vol. 82, no. 24, p. 245207, 2010.

[45] Z. Tang *et al.*, "Relating open-circuit voltage losses to the active layer morphology and contact selectivity in organic solar cells," *J. Mater. Chem. A*, vol. 6, no. 26, pp. 12574–12581, 2018.

[46] Y. Terao, H. Sasabe, and C. Adachi, "Correlation of hole mobility, exciton diffusion length, and solar cell characteristics in phthalocyanine/fullerene organic solar cells," *Appl. Phys. Lett.*, vol. 90, no. 10, p. 103515, 2007.

[47] A. Armin *et al.*, “Quantum Efficiency of Organic Solar Cells: Electro-Optical Cavity Considerations,” *ACS Photonics*, vol. 1, no. 3, pp. 173–181, 2014.

[48] S.-B. Rim, R. F. Fink, J. C. Schöneboom, P. Erk, and P. Peumans, “Effect of molecular packing on the exciton diffusion length in organic solar cells,” *Appl. Phys. Lett.*, vol. 91, no. 17, p. 173504, 2007.

[49] B. Qi and J. Wang, “Open-circuit voltage in organic solar cells,” *J. Mater. Chem.*, vol. 22, no. 46, pp. 24315–24325, 2012.

[50] H. Unay *et al.*, “Benzotriazole and benzodithiophene containing medium band gap polymer for bulk heterojunction polymer solar cell applications,” *J. Polym. Sci. Part A Polym. Chem.*, vol. 53, no. 4, pp. 528–535, 2014.

[51] J. Yuan *et al.*, “Incorporation of Fluorine onto Different Positions of Phenyl Substituted Benzo[1,2-b:4,5-b′]dithiophene Unit: Influence on Photovoltaic Properties,” *Macromolecules*, vol. 48, no. 13, pp. 4347–4356, 2015.

[52] Z. Cong *et al.*, “Alternating polymers based on fluorinated alkoxyphenyl-substituted benzo[1,2-b:4,5-b′]dithiophene and isoindigo derivatives for polymer solar cells,” *Dye. Pigment.*, vol. 146, pp. 529–536, 2017.

[53] J. Shin, M. Kim, J. Lee, H. G. Kim, H. Hwang, and K. Cho, “Positional effects of fluorination in conjugated side chains on photovoltaic properties of donor-acceptor copolymers,” *Chem. Commun.*, vol. 53, no. 6, pp. 1176–1179, 2017.

[54] S. Li *et al.*, “Synthesis, characterization and photovoltaic performances of D-A copolymers based on BDT and DBPz: The largely improved performance caused by additional thiophene blocks,” *J. Mater. Chem. A*, vol. 1, no. 14, pp. 4508–4515, 2013.

[55] R. Kroon, M. Lenes, J. C. Hummelen, P. W. M. Blom, and B. De Boer, “Small bandgap polymers for organic solar cells (polymer material development in the last 5 years),” *Polym. Rev.*, vol. 48, no. 3, pp. 531–582, 2008.

[56] N. K. Elumalai and A. Uddin, “Open circuit voltage of organic solar cells: An

in-depth review," *Energy Environ. Sci.*, vol. 9, no. 2, pp. 391–410, 2016.

[57] A. A. B. Alghamdi *et al.*, "Selenophene vs. thiophene in benzothiadiazole-based low energy gap donor–acceptor polymers for photovoltaic applications," *J. Mater. Chem. A*, vol. 1, no. 16, pp. 5165–5171, 2013.

[58] J. M. Chem, H. Chen, S. Yeh, C. Chen, and C. Chen, "Comparison of thiophene- and selenophene-bridged donor – acceptor low band- gap copolymers used in bulk-heterojunction organic photovoltaics †," *J. Mater. Chem.*, vol. 22, no. 40, pp. 21549–21559, 2012.

[59] I. Onk, G. Hizalan, Ş. Cevher, S. Hacioglu, L. Toppare, and A. Cirpan, "Multipurpose selenophene containing conjugated polymers for optoelectronic applications," *J. Macromol. Sci. Part A*, vol. 54, pp. 133–139, 2017.

[60] V. Cuesta *et al.*, "Increase in efficiency on using selenophene instead of thiophene in π-bridges for D-π-DPP-π-D organic solar cells," *J. Mater. Chem. A*, vol. 7, no. 19, pp. 11886–11894, 2019.

[61] G. Hızalan, A. Balan, D. Baran, and L. Toppare, "Spray processable ambipolar benzotriazole bearing electrochromic polymers with multi-colored and transmissive states," *J. Mater. Chem.*, vol. 21, no. 6, pp. 1804–1809, 2011.

[62] M. Yuan, P. Yang, M. M. Durban, and C. K. Luscombe, "Low Bandgap Polymers Based on Silafluorene Containing Multifused Heptacylic Arenes for Photovoltaic Applications," *Macromolecules*, vol. 45, no. 15, pp. 5934–5940, 2012.

[63] A. Moulé, J.-B. Bonekamp, and K. Meerholz, "The effect of active layer thickness and composition on the performance of bulk-heterojunction solar cells," *J. Appl. Phys.*, vol. 100, 2006.

APPENDICES

A. NMR DATA

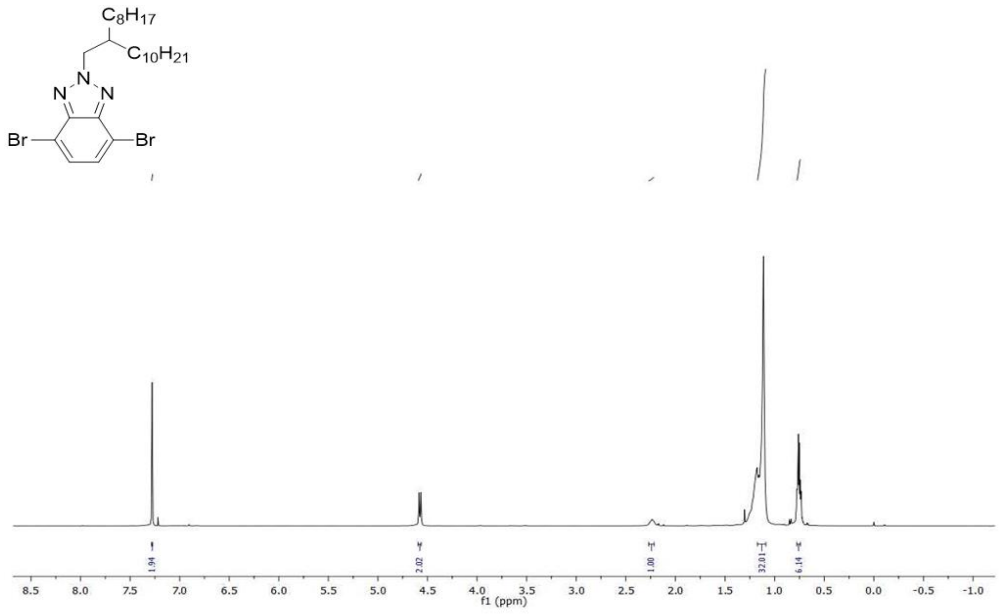

Figure A.1. ^{1}H NMR result of Compound 6

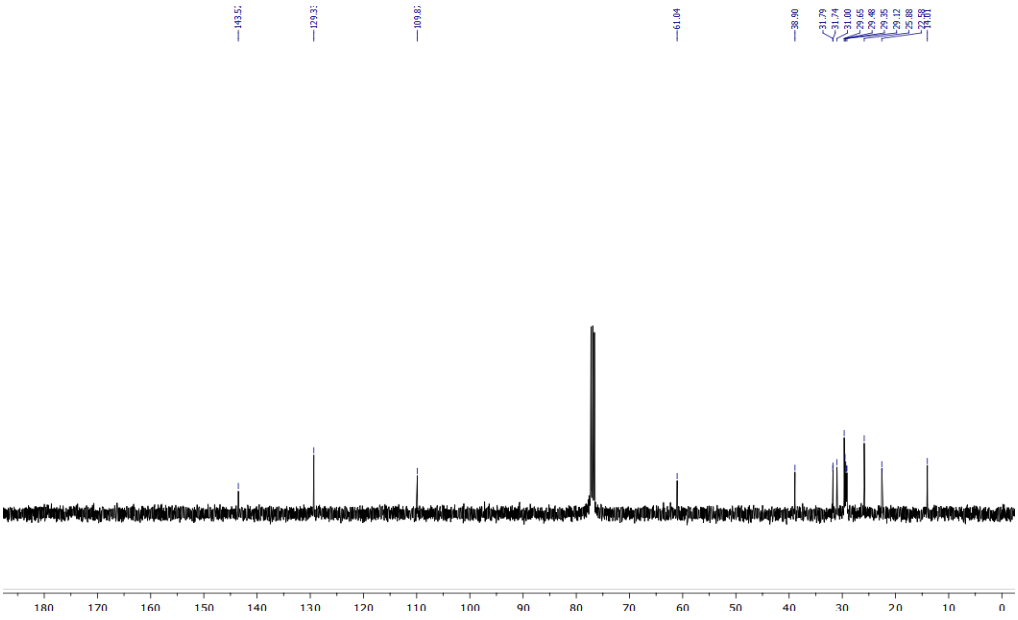

Figure A.2. ^{1}H NMR result of Compound 6

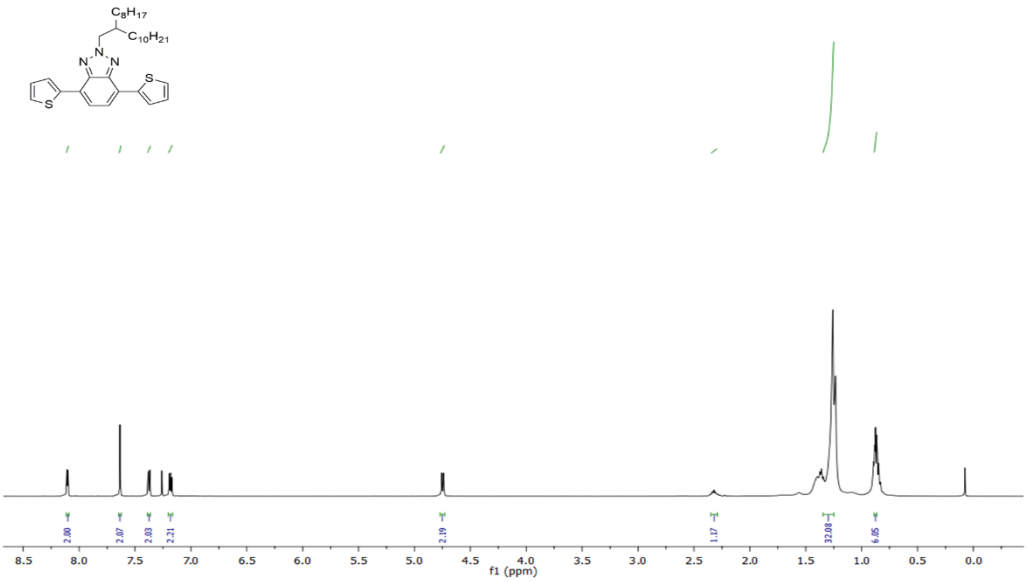

Figure A.3. ^{1}H NMR result of Compound 9

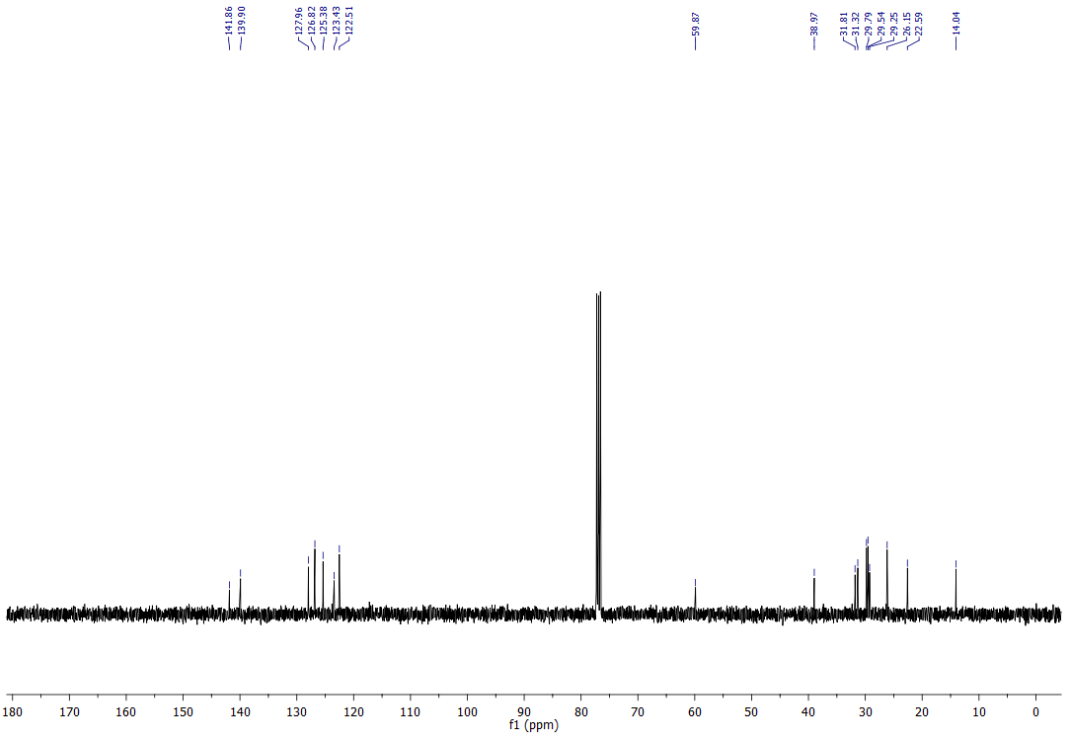

Figure A.4. ^{13}C NMR result of Compound 9

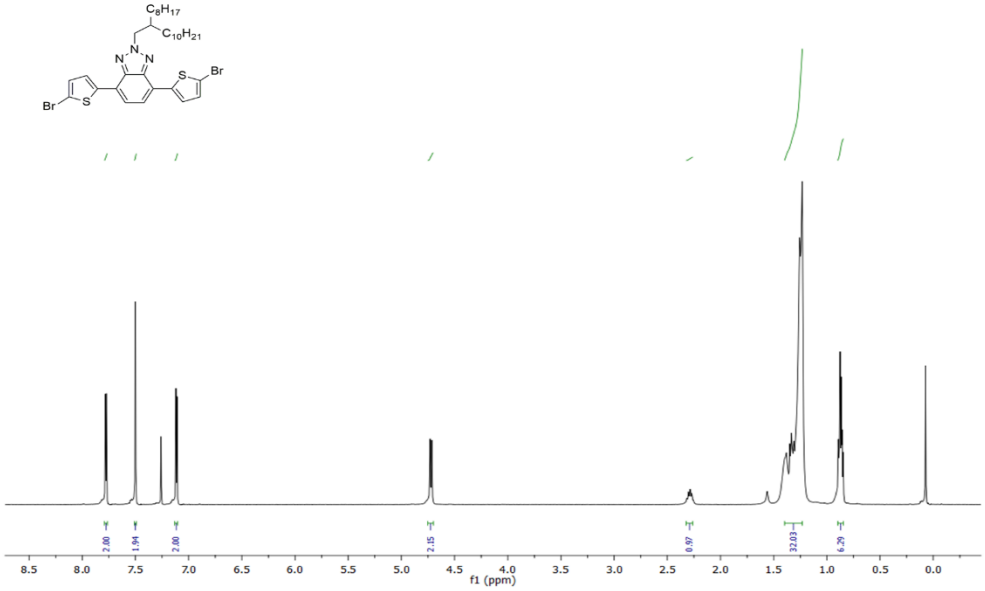

Figure A.5. ^{1}H NMR result of Compound 10

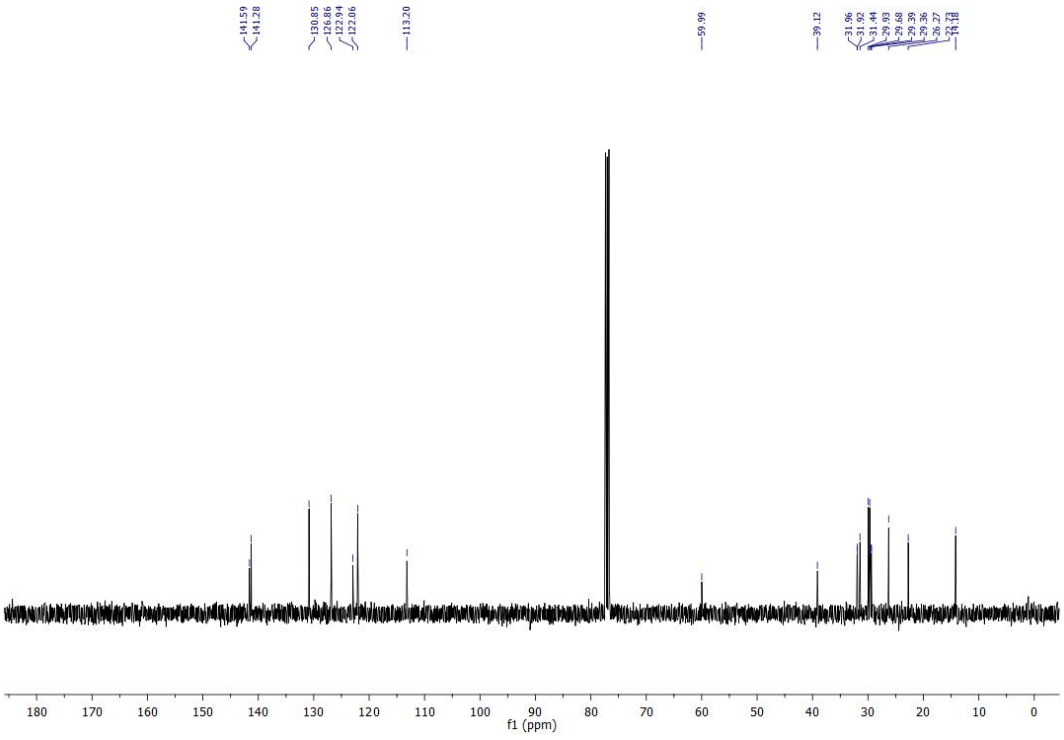

Figure A.6. ^{13}C NMR result of Compound 10

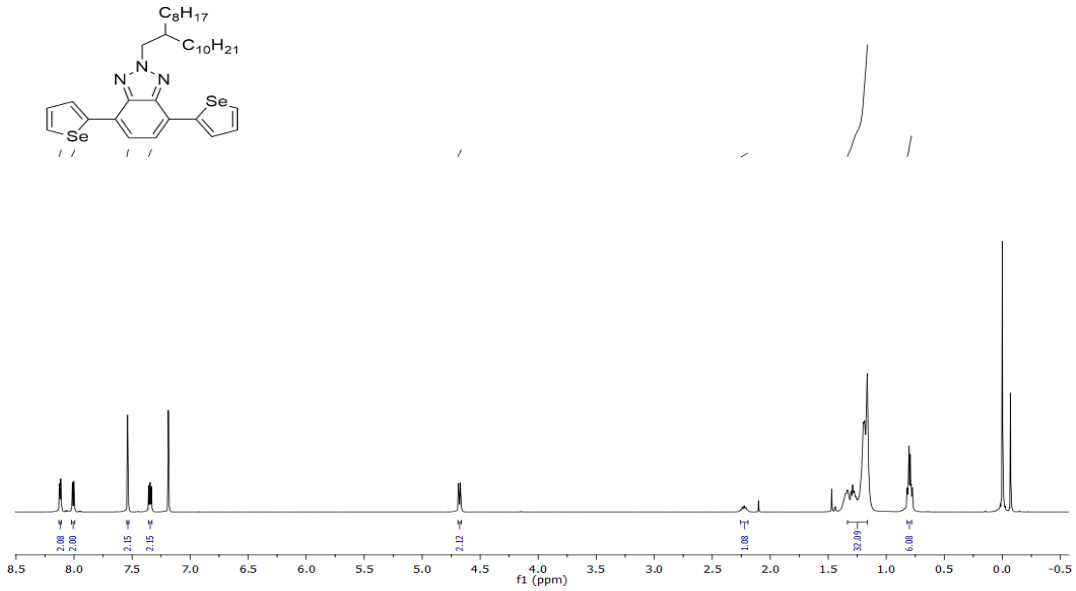

Figure A.7. ^{1}H NMR result of 13

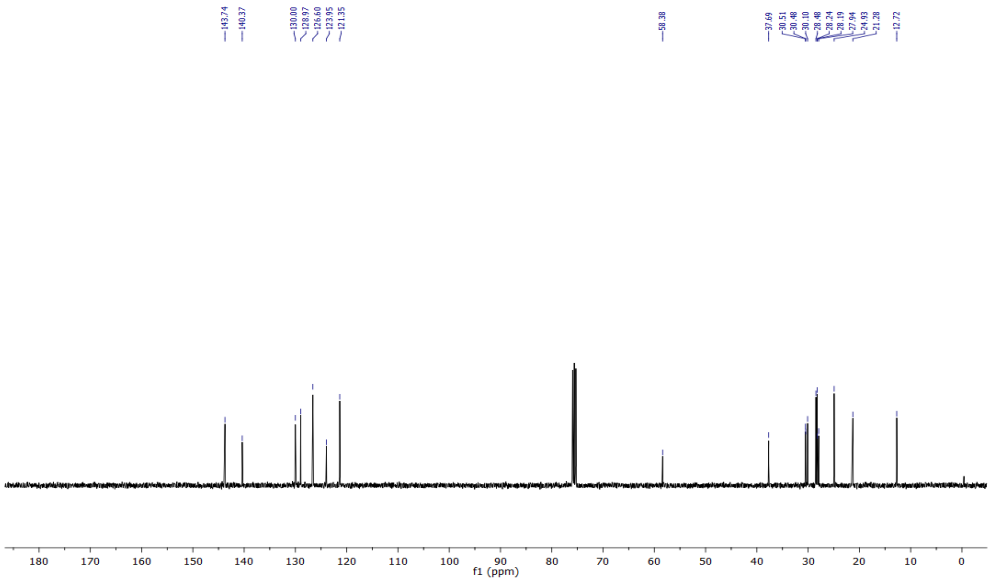

Figure A.8. ^{13}C NMR result of 13

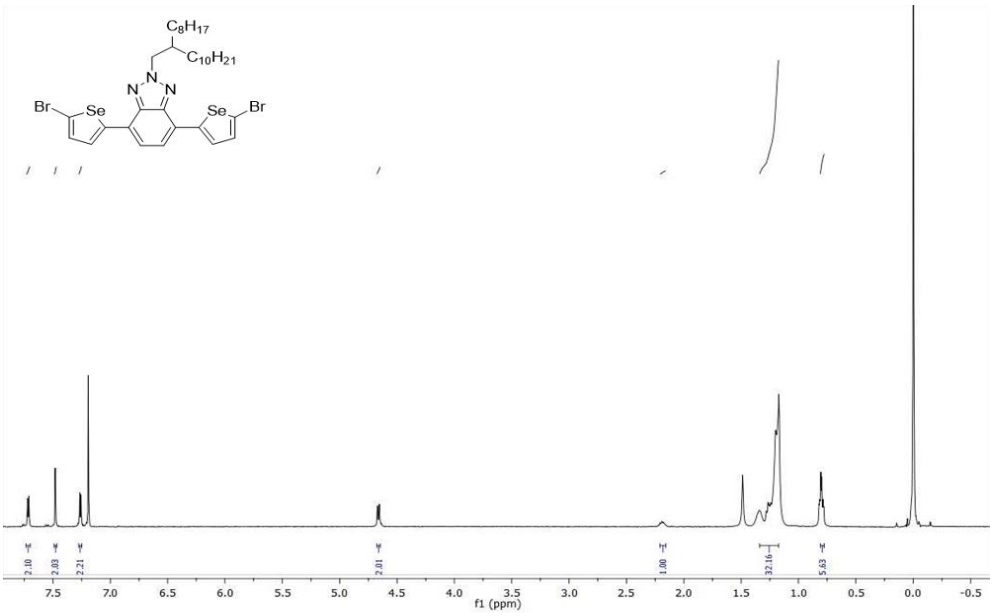

Figure A.9. ^{1}H NMR result of Compound 14

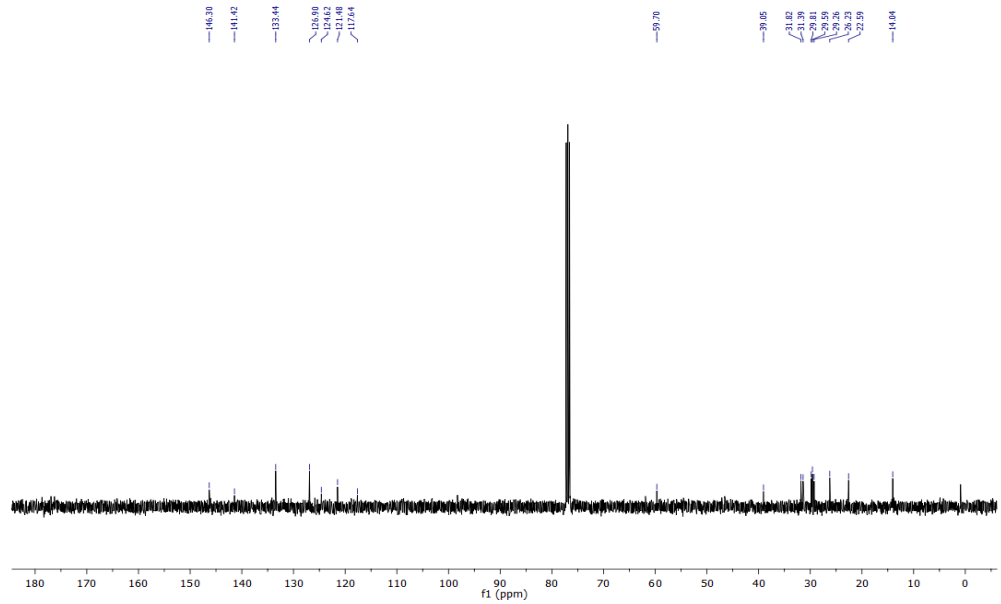

Figure A.10. ^{13}C NMR result of Compound 14

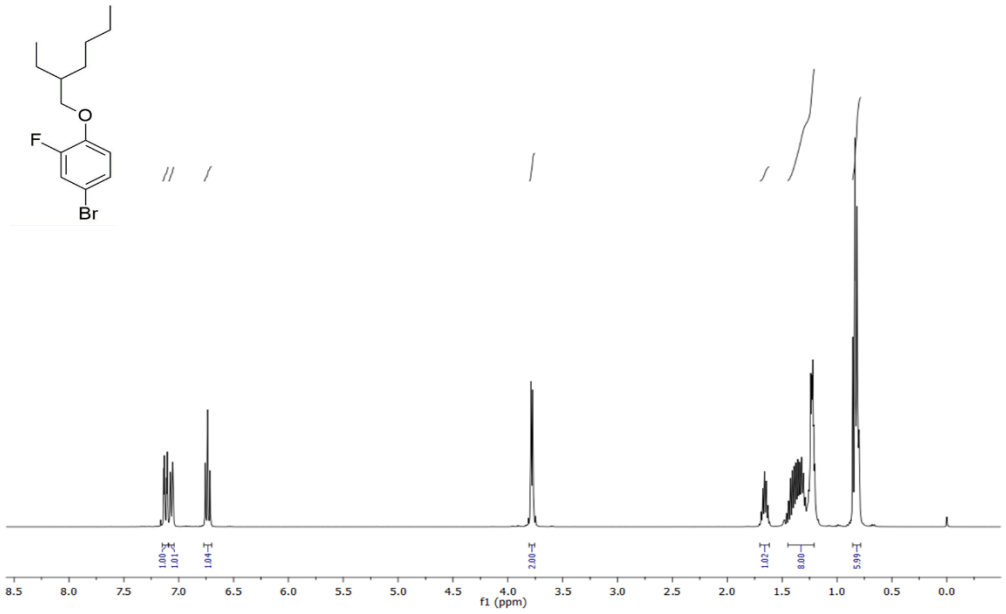

Figure A.11. ^{1}H NMR result of Compound 16

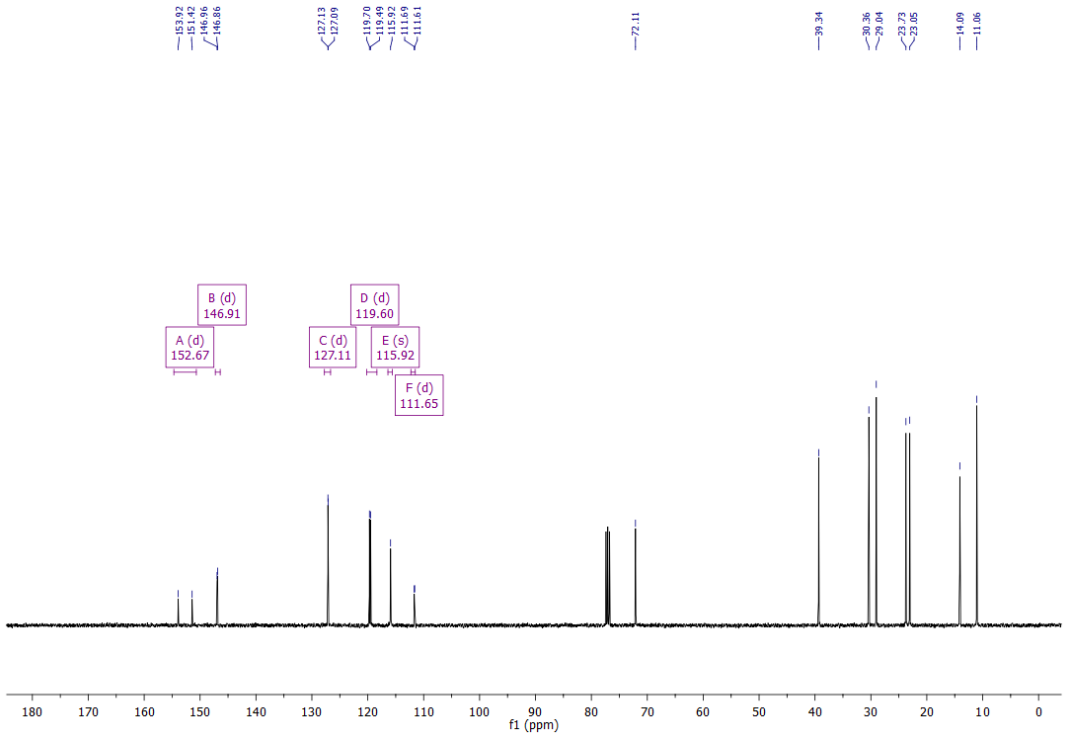

Figure A.12. ^{13}C NMR result of Compound 16

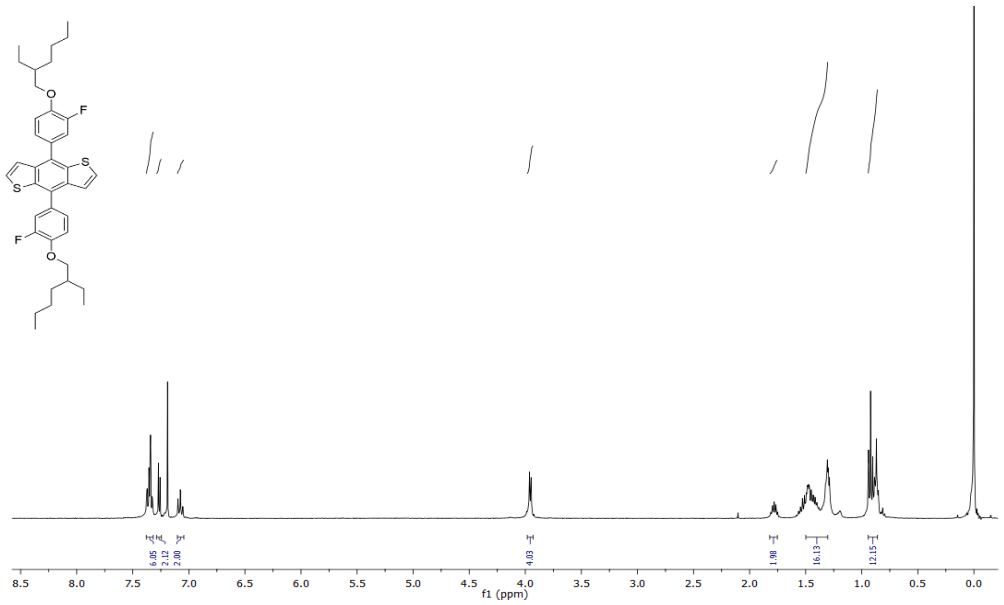

Figure A.13. ^{1}H NMR result of Compound 18

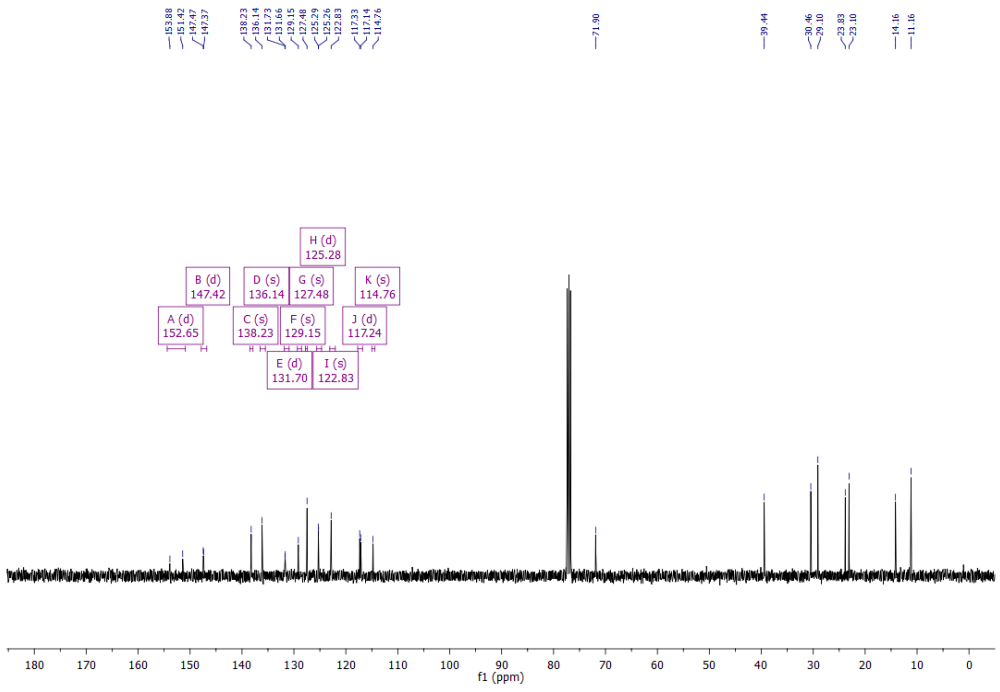

Figure A.14. ^{13}C NMR result of Compound 18

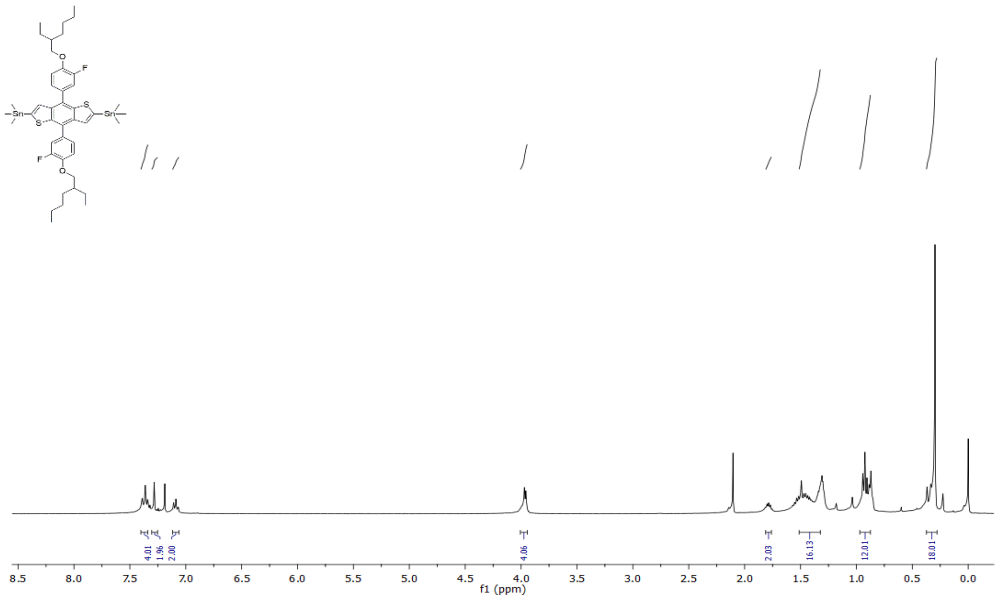

Figure A.15. ^{1}H NMR result of Compound 19

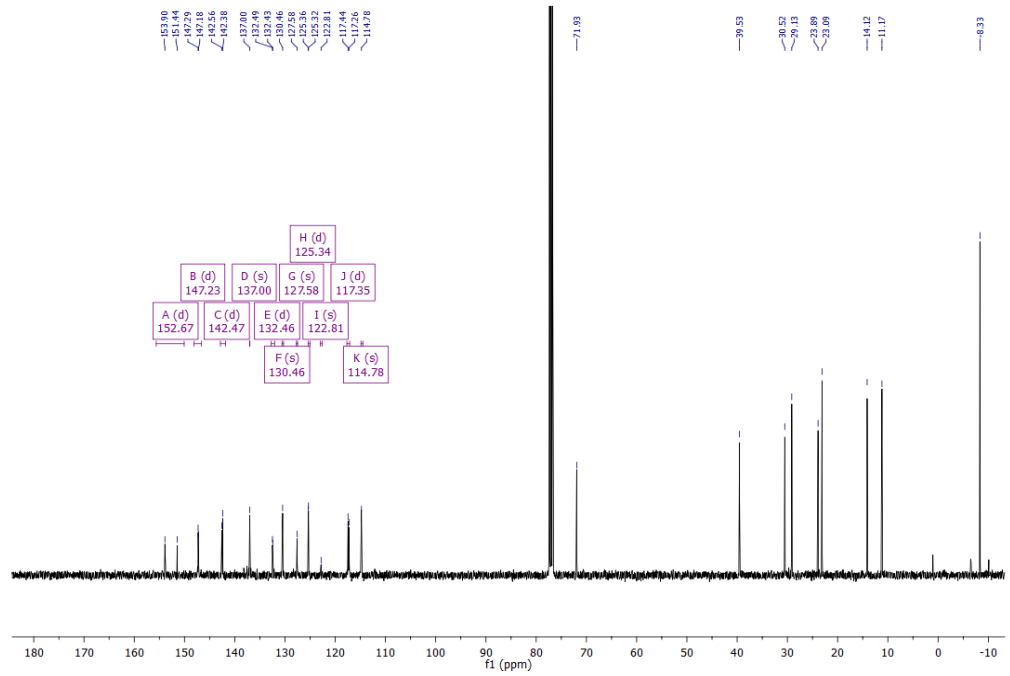

Figure A.16. ^{13}C NMR result of Compound 19

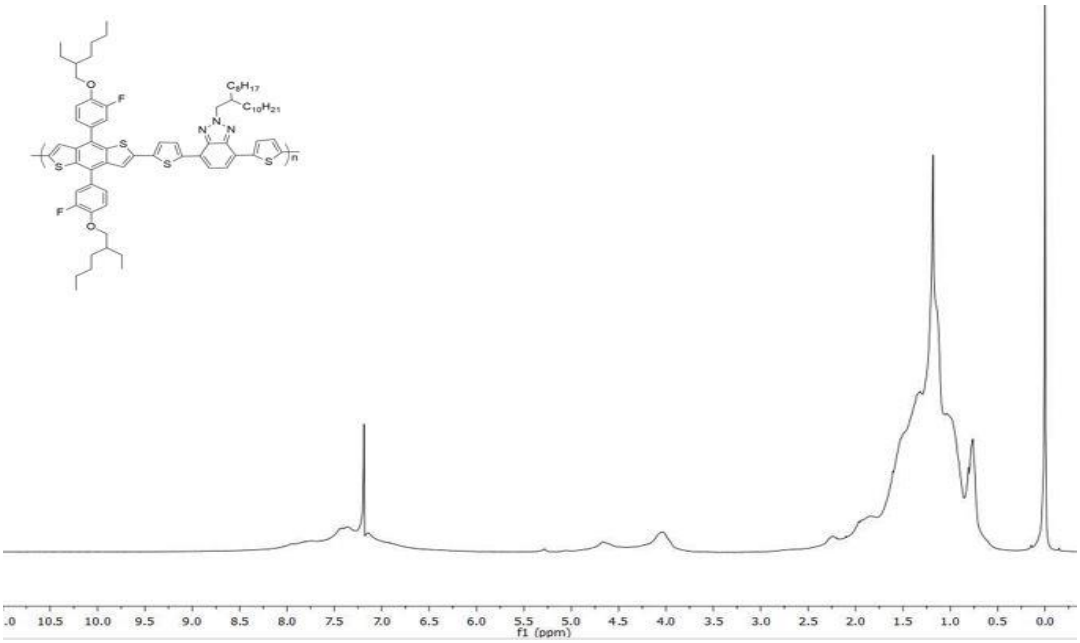

Figure A.17. ^{1}H NMR result of P1

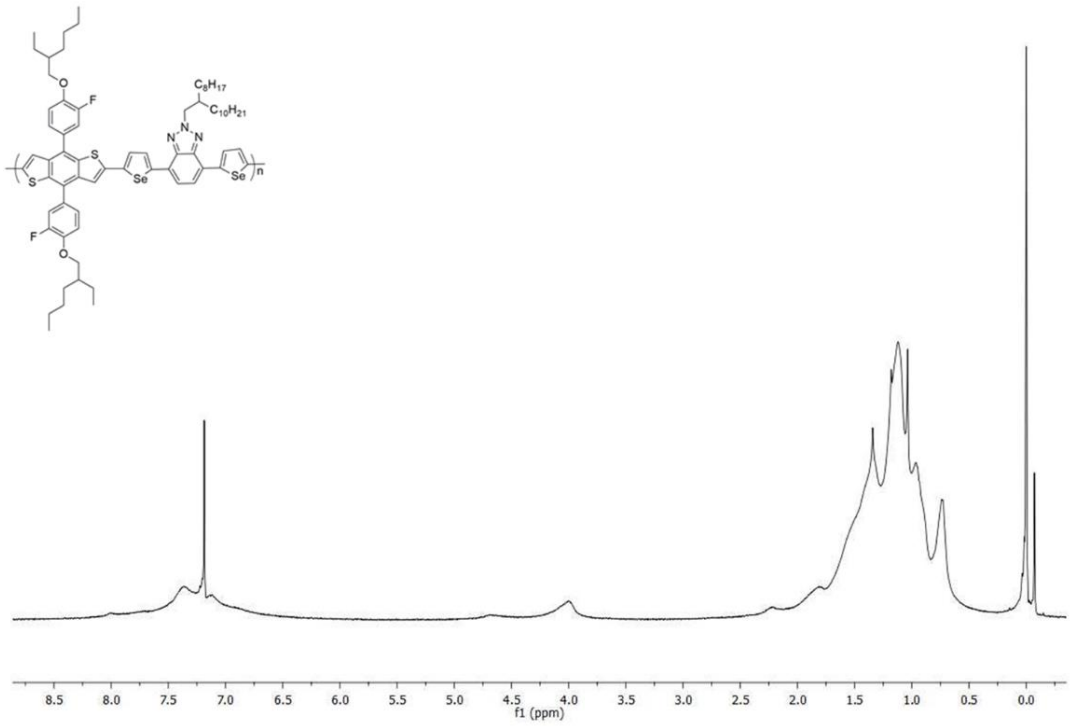

Figure A.18. ^{1}H NMR result of P2

B. THERMAL ANALYSIS RESULTS

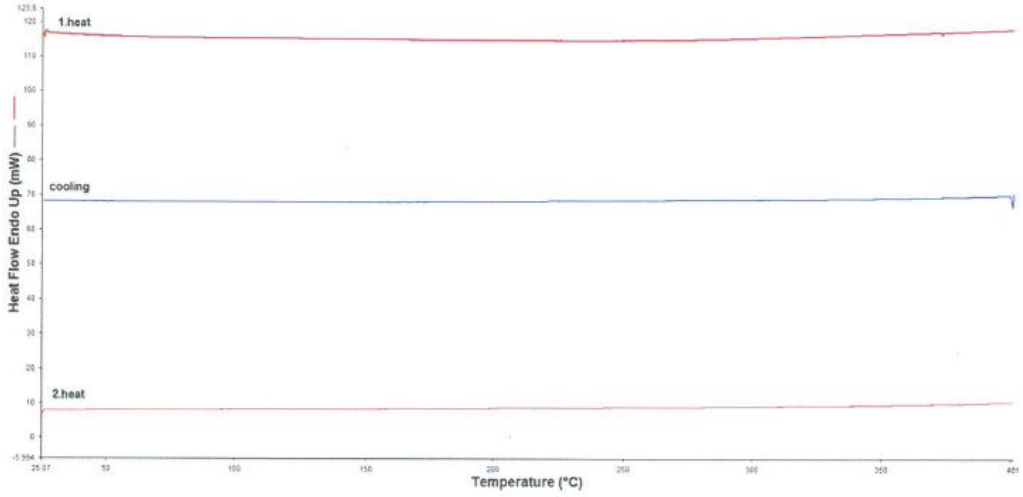

Figure B.1. DSC Thermogram of P1

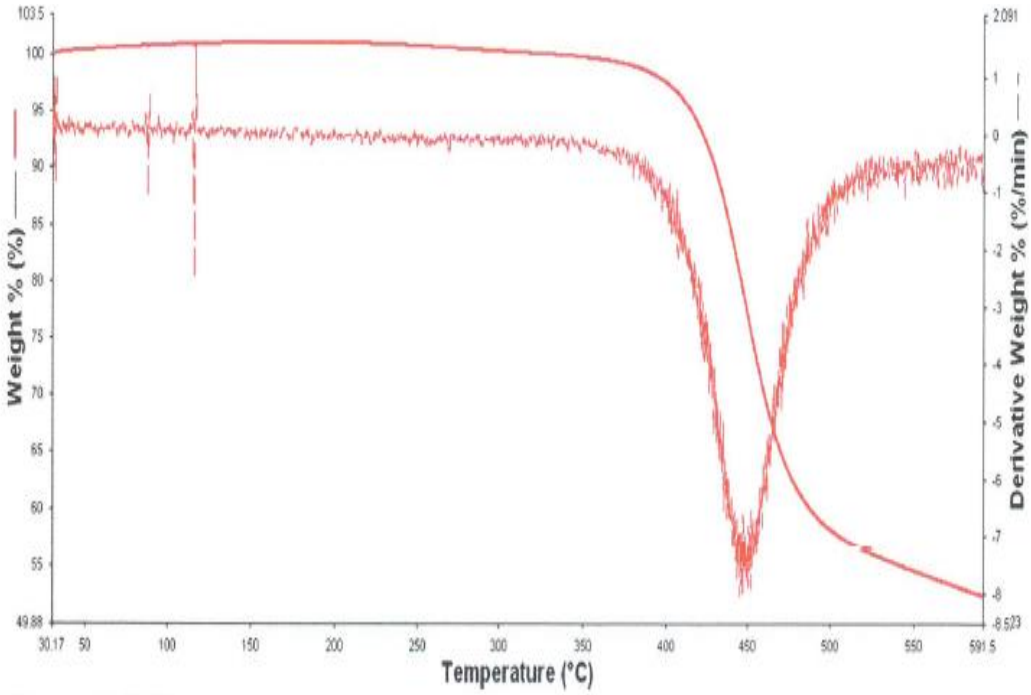

Figure B.2. TGA Curve of P1

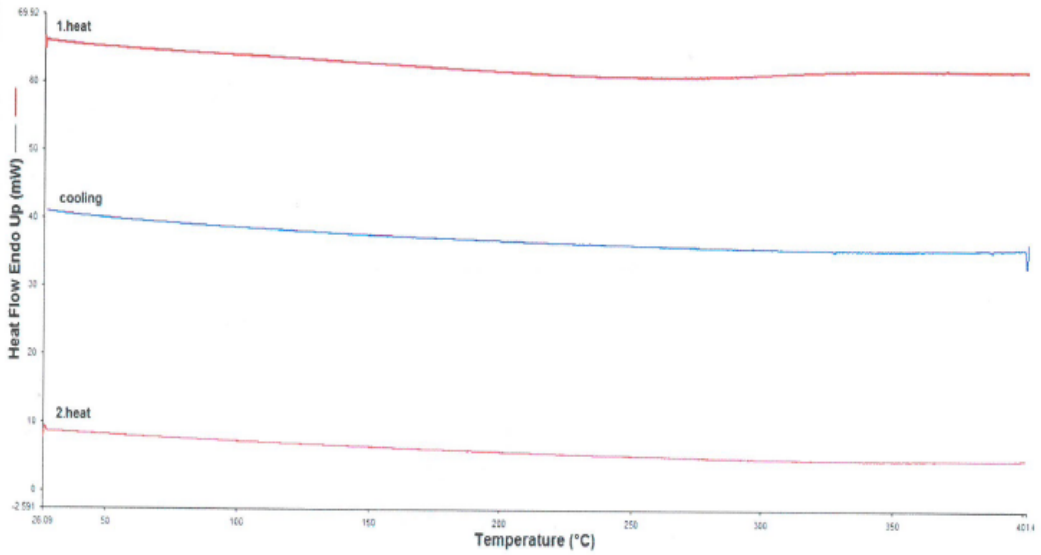

Figure B.3. DSC Thermogram of P2

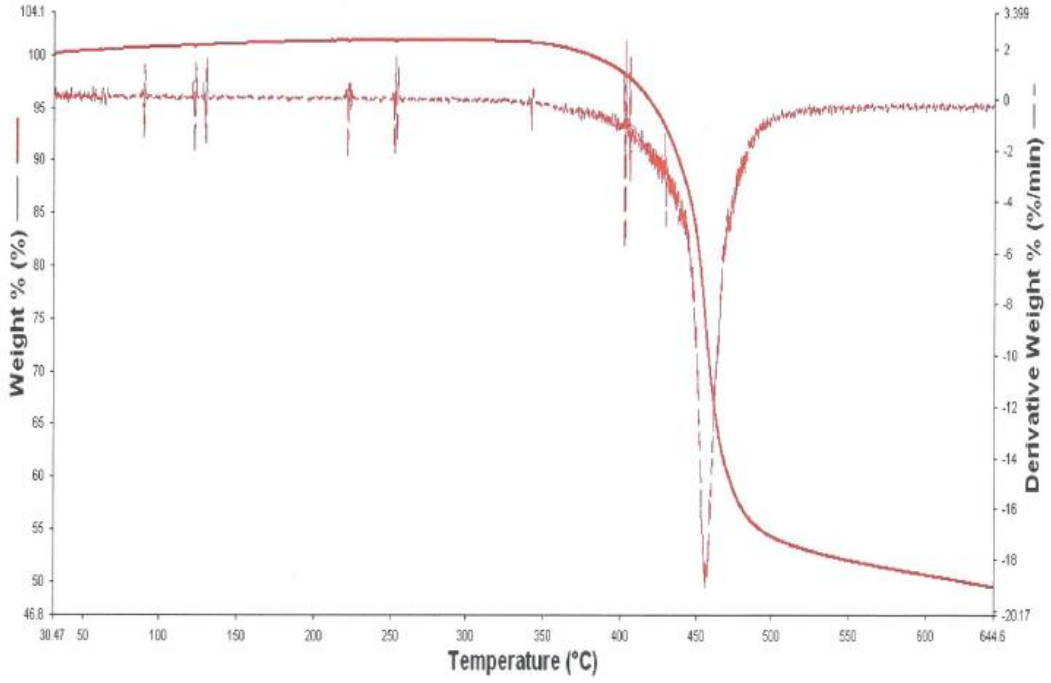

Figure B.4. TGA Curve of P2